ACS APPLIED MATERIALS & INTERFACES

www.acsami.org

Review

Harvesting Water Energy through the Liquid−Solid Triboelectrification

Peng Cheng, Yang Zou,* and Zhou Li*

Cite This: ACS Appl. Mater. Interfaces 2024, 16, 47050−47074

Read Online

ACCESS | Metrics & More | Article Recommendations

ABSTRACT: The escalating energy and environmental challenges have catalyzed a global shift toward seeking more sustainable, economical, and eco-friendly energy solutions. Water, capturing 35% of the Earth's solar energy, represents a vast reservoir of clean energy. However, current industrial capabilities harness only a fraction of the energy within the hydrological cycle. The past decade has seen rapid advancements in nanoscience and nanomaterials leading to a comprehensive exploration of liquid−solid triboelectrification as a low-carbon, efficient method for water energy harvesting. This review explores two fundamental principle models involved in liquid−solid triboelectrification. On the basis of these models, two distinct types of water energy harvesting devices, including droplet-based nanogenerators and water evaporation-induced nanogenerators, are summarized from their working principles, recent developments, materials, structures, and performance optimization techniques. Additionally, the applications of these nanogenerators in energy harvesting, self-powered sensing, and healthcare are also discussed. Ultimately, the challenges and future prospects of liquid−solid triboelectrification are further explored.

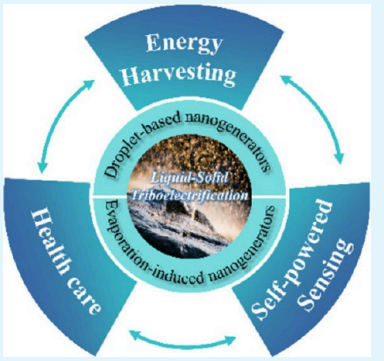

KEYWORDS: *liquid−solid triboelectrification, nanogenerators, droplet-based, evaporation-induced, energy harvesting, self-powered sensing*

1. INTRODUCTION

Entering the 21st century, the depletion of fossil fuels and escalating environmental issues have emerged as significant global challenges, pressing the need for cleaner, renewable energy sources and methods to mitigate environmental impacts. Encompassing 71% of the Earth's surface, water plays a pivotal role in the global ecosystem, driven by the dynamic hydrological cycle involving evaporation, condensation, precipitation, surface runoff, and groundwater flow. This cycle serves as a rich source of thermal, chemical, and kinetic energy throughout its various phases of transition and movement.[1,2] The strategic harnessing of this vast, untapped energy reserve is crucial for mitigating the global energy crisis, drawing the focused efforts of researchers worldwide.

Currently, hydroelectric power stations utilizing electromagnetic generators have maximized the exploitation of kinetic energy within the hydrological cycle. Yet, the inherent constraints posed by these stations' geographic locations and the generators' principles, favoring high-frequency, large-amplitude, and robust mechanical power outputs, render the nuanced energy of water—such as the low-frequency and minimal mechanical power in water droplets and evaporation—largely untapped. Many new technologies have been developed to harness the weak, scattered energy in water, such as reverse electrodialysis,[3−5] moisture-based power generation and so on.[6−8] However, due to various reasons, such as the need for high-performance ion exchange membranes for reverse electrodialysis and the limited sustainability of moisture-based power generation, their applications face significant challenges. Introduced by Zhonglin Wang and his team in 2012, Triboelectric Nanogenerators (TENGs) offer a paradigm shift.[9] Merging contact electrification with electrostatic induction, TENG harnesses the friction potential to transform mechanical energy into electrostatic energy, subsequently generating electricity via external circuit charge flow. TENGs are characterized by affordability, diverse material compatibility and an aptitude for harvesting ultralow frequency and atypical mechanical energies.[10−14] The contact electrification extends beyond solid−solid interfaces to include solid−liquid and solid−gas interactions, such as those involving raindrops or sand particles in air.[15,16] In the past decade, due to the rapid development of nanomaterials, solid−liquid contact electrification has been extensively studied. Based on it, two liquid−solid triboelectrification-based nanogenerators, the droplet-based nanogenerators and the evaporation-induced nanogenerators, were invented and applied to

Received: June 14, 2024
Revised: August 21, 2024
Accepted: August 24, 2024
Published: August 29, 2024

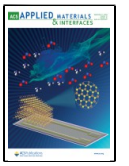

https://doi.org/10.1021/acsami.4c09044
ACS Appl. Mater. Interfaces 2024, 16, 47050−47074

harvesting water energy, attracting the interest of researchers around the world.

Recently, some reviews on the topic of water energy harvesting have been published.[17−22] These articles mainly focus on harvesting various forms of water energy, such as wave energy and droplet energy, or summarizing specific power generation methods from their mechanisms to applications, such as droplet-based nanogenerators and moisture-based power generation with summarizing their applications into two major aspects: power sources and sensors. For example, the review by Guo et al. provides a comprehensive overview of the research progress of hydropower generation,[17] and Yang et al. review the progress of droplet-based nanogenerators from various principles and structures.[20] In this review, the focus is on liquid−solid triboelectrification, based on which the latest progress in harnessing water energy is deeply explored. Initially, it delineates Wang's transition theory on contact electrification alongside a novel two-step model for the genesis of the electric double layer (EDL) at the liquid−solid interface. Following that, because the working modes of droplet-based nanogenerators are closely related to their working principle and application scenarios, the paper delves into the latest developments in three modes of droplet-based nanogenerators. Differently, as evaporation-induced nanogenerators involve complex solid−liquid interfaces and the characteristics of nanomaterials, the material selection, device structures, and performance optimization strategies of evaporation-induced nanogenerators are further reviewed. Additionally, this review also shines a light on the practical applications of liquid−solid triboelectrification-based nanogenerators, ranging from energy harvesting and self-powered sensing to healthcare solutions, with concluding the potential and directions for future application.

2. PRINCIPLE OF LIQUID−SOLID TRIBOELECTRIFICATION

2.1. Wang's Transition Model. Triboelectrification (TE), a cohesive process intertwining tribology with interface charge transfer, is scientifically categorized as contact electrification (CE), which has been documented extensively throughout history. TE is characterized by its ubiquity, capable of occurring at any moment across a diverse array of materials, encompassing all recognized solids, liquids, and gases. Despite TE's fundamental nature and widespread occurrence, the intricacies of its underlying physical mechanism remain minimally understood. The complexity of TE's physical processes continues to be a subject of significant scientific inquiry.

In prior research, it has been suggested that triboelectrification (TE) arises from the transfer of electrons,[23−25] ions,[26] and even entire materials.[27,28] Given the constraints of existing research methodologies, a multitude of materials have been observed to exhibit the TE phenomenon, leading to a broad spectrum of conclusions. However, not all findings are universally applicable across different scenarios. In contrast, the advent of triboelectric nanogenerators (TENGs) by Wang's team in 2012 marked a significant breakthrough. These devices are capable of efficiently transforming irregular, low-frequency mechanical energy into electrical energy, drawing widespread interest in recent years.[29−31] The principle of triboelectrification underpins the fundamental operation of TENGs, facilitating the conversion of external mechanical energy into internal electrostatic energy. This energy is then converted into electrical output in the external circuit through electrostatic induction. To provide a robust scientific foundation for TENGs and enhance their performance, Wang introduced the Wang's transition model of TE,[16] as depicted in Figure 1.

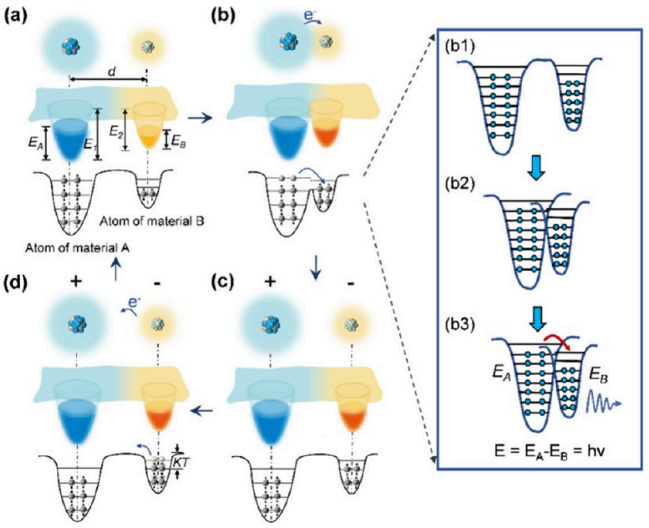

Figure 1. Wang's transition model of triboelectrification. Schematic diagram of the electron cloud and potential energy distribution diagram of two atoms belonging to two materials respectively before (a) contact, (b) during contact, and (c) after contact indicating that electrons are transferred from one atom to another after strong electron cloud overlap occurs. (d) The charge released at high temperature when KT approaches the barrier height. d represents the distance between the two nuclei; E_A and E_B represent the occupied energy levels of the electrons; E_1 and E_2 represent the potential energy of the electrons escaping. (b1−b3) A detailed illustration of (b) to illustrate that electron cloud overlap leads to a lowering of the potential barrier between two atoms, resulting in interatomic electronic transitions and possible photon emission. Reproduced with permission from ref 14. Copyright 2018 WILEY-VCH Verlag GmbH & Co. KGaA, Weinheim.

As shown in Figure 1a, prior to atomic-scale interaction between the two materials, their electron clouds remain distinct and nonoverlapping, with the potential wells securely anchoring electrons within specific orbits to inhibit free escape. At this juncture, the atoms exhibit mutual attraction. The energy levels occupied by electrons are denoted as E_A and E_B, whereas E_1 and E_2 represent the potential energies required for electron escape, with d indicating the internuclear distance. Upon the atoms of both materials approaching proximity and the application of external pressure, d diminishes to below the equilibrium distance necessary for the formation of ionic or covalent bonds, thereby entering an exclusion zone. Consequently, a significant overlap of electron clouds occurs, transitioning the initial singular potential well into an asymmetric double potential well. This transition results in a reduced energy barrier, facilitating electron transfer from one atom to another, culminating in contact electrification (CE) as illustrated in Figure 1b. Figure b1-b3 elucidate how the overlap of electron clouds contributes to the reduction of the barrier, prompting electron transitions between atoms and the potential for photon emission.[32] Following the separation of the material (Figure 1c), the electrons that were transferred persist on the material surface as electrostatic charges. While

https://doi.org/10.1021/acsami.4c09044
ACS Appl. Mater. Interfaces 2024, 16, 47050−47074

theory posits that the electrostatic charge induced by CE should remain on the surface for an extended duration, empirical evidence suggests that the frictional charge at elevated temperatures adheres to the principle of hot electron emission, when the thermal energy (KT) approaches the barrier height, the atoms release the frictional charge at high temperatures (Figure 1d).[33,34]

The Wang's transition model received strong experimental support upon its proposal. In their research, the charge transfer in contact electrification (CE) was quantitatively studied with triboelectric nanogenerators, analyzing its real-time variation with temperature. Based on the experimental results, the aforementioned electron-cloud-potential well model was proposed, which can be widely applied to explain all types of CE in conventional materials.[23] Moreover, in their subsequent research, this electron transfer-dominated contact electrification mechanism has received even broader experimental support.[35,36] Based on the Wang's transition model, liquid−solid triboelectrification occurs through electron transfer due to the strong overlap of electron clouds. Subsequently, in the droplet-based nanogenerators, liquid−solid triboelectrification converts the kinetic energy of the droplet into electrical energy through coupling with electrostatic induction phenomenon, which is also a prerequisite for the formation of an electric double layer (EDL) in the evaporation-induced nanogenerators.

2.2. Wang's Hybrid EDL Model. Wang's transition model delineates an electron-cloud-potential well framework that elucidates the charge transfer mechanics inherent to triboelectrification (TE) across various material interactions. This model is adept at explaining TE phenomena occurring between combinations of solid−solid, solid−liquid, solid−gas, and even liquid−liquid interfaces. A well-known phenomenon is that an EDL will form on solid surface upon contact with liquid. The consensus on EDL composition includes a Stern layer, which is an inner layer tightly adsorbed onto the solid surface, and a diffusion layer constituting the outer segment.[37,38] Despite the established fact of its existence and well-defined structure, the transition process from the initial contact with the liquid to the full formation of EDL remains somewhat ambiguous. To bridge this gap, Wang's team introduced a hybrid EDL theory, rooted in Wang's transition model, as illustrated in Figure 2.[16]

The formation process of the EDL is categorized into two steps. Initially, upon the first instance of liquid molecules making contact with the wall, the wall is devoid of any surface charge (Figure 2a). According to the Wang's transition model, the atomic interaction between the liquid and solid leads to a significant overlap of electron clouds and subsequent electron transfer, thereby charging the previously neutral atoms on the solid surface (Figure 2b). Following this, the mechanical action induced by liquid flow propels the molecules that have undergone electron transfer, along with other molecules, away from the solid wall, consequently depositing a layer of ions on the solid surface (Figure 2c and 2d). In the subsequent step, should the solution contain free ions, such as H^+ and OH^-, the counterions dispersed within the solution are drawn toward the solid charged surface through Coulomb force. This interaction culminates in the formation of a fixed layer (Stern layer) alongside a diffusion layer, thereby establishing the EDL (Figure 2e). This hybrid EDL theory deviates from traditional EDL theories by highlighting the pivotal role of electron transfer in creating the initial charged state on the solid surface. The EDL thus formed aligns with numerous

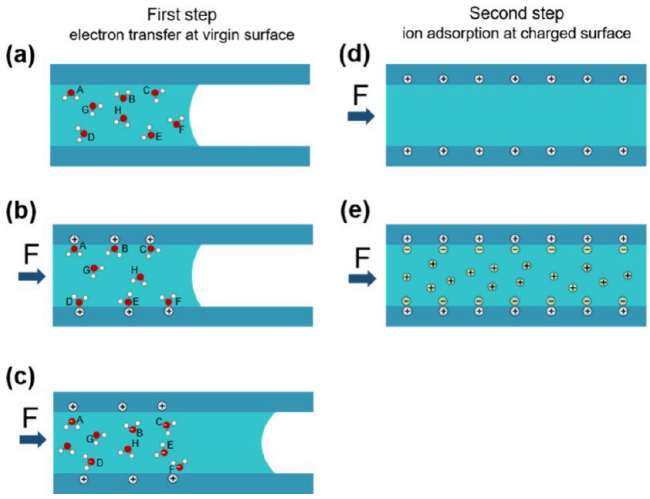

Figure 2. Two steps of hybrid EDL theory. In the first step, the liquid and the solid surface come into contact at the atomic level and the electron clouds strongly overlap, thereby causing the electrons transfer. In the second step, the counterions in the solution are attracted by Coulomb force to form a Stern layer and a diffusion layer. Reproduced with permission from ref 16. Copyright 2019 Elsevier.

studies and models concerning potential distribution and surface chemistry documented in scientific literature.[39−41]

After the solid−liquid interface electric double layer is formed based on the hybrid EDL theory, when the solution is confined in a nanoscale channel, such as in graphene oxide, the EDL will overlap significantly, resulting in a confined solution dominated by counterions. The fluid motion driven by pressure or gravity will lead to the directional movement of counterions in the diffusion layer. The continuous accumulation of counterions can generate stable electric potential at both ends of the channel, thus converting potential energy and kinetic energy into electric energy, which is the working principle of the evaporation-induced nanogenerators recognized by most researchers at present.[42−46]

3. DROPLET-BASED NANOGENERATORS

As they fall from the sky in the form of rain, water droplets not only gain significant kinetic energy but also gather electrostatic energy due to the triboelectrification process with air, a primary factor contributing to thunderstorms. The annual global rainfall amounts to about 500,000 cubic kilometers, with water droplets harboring up to 3,000 TW h of energy every year.[47] Fully harnessing this energy could substantially reduce energy pressures. Recently, due to their low cost, simplicity in manufacturing, and high energy conversion efficiency, droplet-based nanogenerators have emerged as a promising solution for capturing the dispersed and low-frequency energy of water droplets.[48−51] Because the working modes of droplet-based nanogenerators are closely related to their working principles and application scenarios, this section mainly introduces the following three types: the single-electrode mode, the free-standing mode, and the transistor-inspired mode. Finally, some emerging technologies that use water droplets to generate electricity will be briefly introduced.

3.1. Single-Electrode Mode Droplet-Based Nanogenerators. The single-electrode mode droplet-based nanogenerators is the first important power generation mode, which was first proposed by Lin et al. in 2014.[52] The working principle of single-electrode mode is shown in Figure 3a,b. The

https://doi.org/10.1021/acsami.4c09044
ACS Appl. Mater. Interfaces 2024, 16, 47050−47074

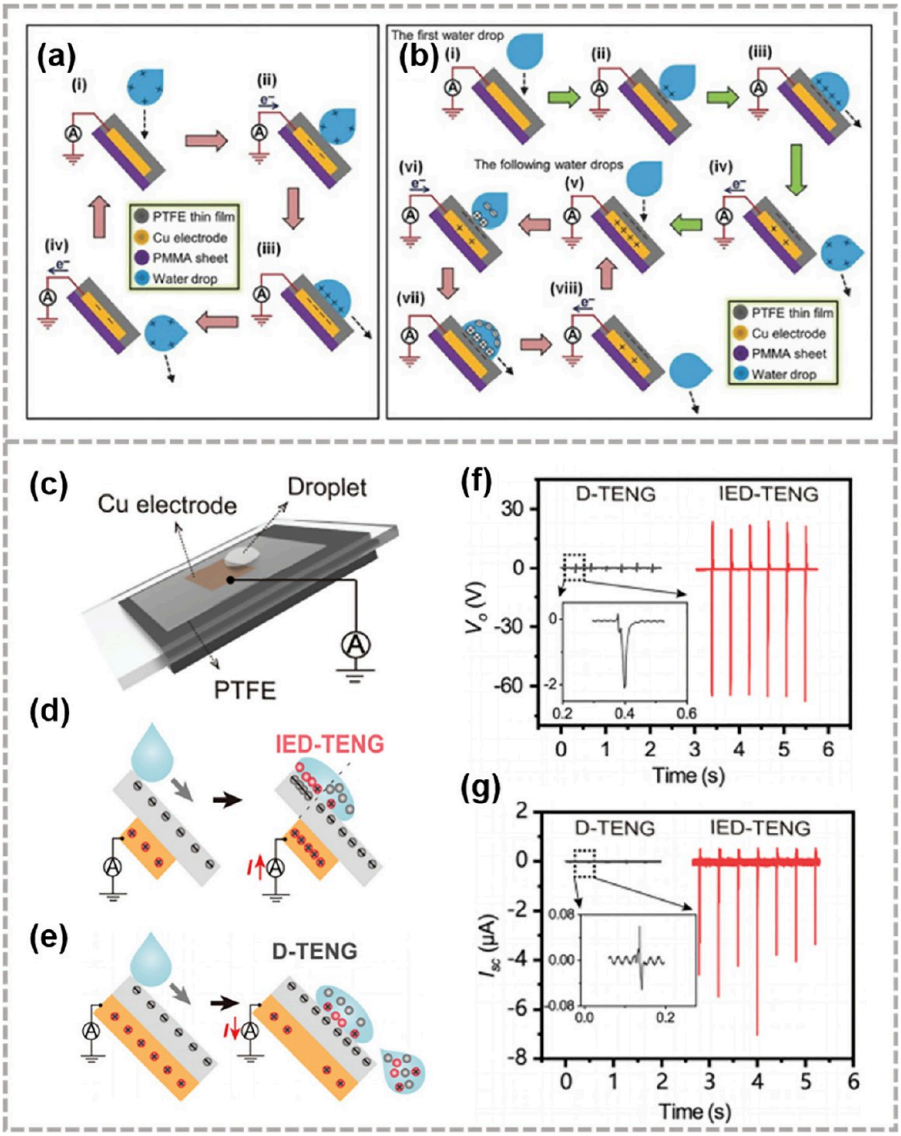

Figure 3. Single-electrode mode droplet-based nanogenerators. (a) The working principle when water droplets are initially charged and (b) not charged. Reproduced with permission from ref 52. Copyright 2014 Wiley-VCH. (c) Induced electric enhanced droplet-based triboelectric nanogenerator (IED-TENG). (d–g) The working diagram and output performance of IED-TENG and traditional single-electrode droplet-based TENG. Reproduced with permission from ref 58. Copyright 2023 Wiley-VCH.

device is composed of poly(methyl methacrylate) (PMMA) substrate, copper electrode and polytetrafluoroethylene (PTFE) friction layer. The copper electrode is grounded through an external circuit. In the single-electrode mode, if the water droplet initially generates frictional charges by rubbing with air or pipe, its working principle is shown in Figure 3a. If the initial water droplet is not charged, the frictional charge is generated when the water droplet slides on the PTFE film, as shown in Figure 3b. In Figure 3a, at stage (i), the device is initially in an electrical equilibrium state, and the surface of water droplet is positively charged due to friction with air or pipes that based on the contact electrification mechanism. When the water droplet impacts the PTFE film, the electrostatic induction phenomenon occurs, and a positive potential difference is generated between the copper electrode and the ground. The electrons are transferred from the ground to the copper electrode to balance the potential difference [Figure 3a(ii)]. Until the droplet diffusion area reaches the maximum, the entire device reaches the electrical equilibrium again, and this process generates an instantaneous positive current [Figure 3a(iii)]. When the water droplet gradually leaves the surface of the PTFE film, the Coulomb force generated by electrostatic induction gradually decreases, and a negative potential difference is generated between the copper electrode and the ground. The electrons flow from the copper electrode to the ground [Figure 3a(iv)] until a new balance [Figure 3a(i)]. This process produces an instantaneous negative current. Continuous AC output can be achieved when the water droplets are continuously dripping.

Figure 3b shows that the water droplet is initially uncharged and falls on the PTFE film to generate frictional charges. Initially, there is no charge in the initial device or the water droplet [Figure 3b(i)]. According to the Wang's transition model, when the water droplet contacts the PTFE film, the electron cloud overlaps strongly at the atomic level, causing electrons to transfer from the atoms in the water to the atoms in the PTFE. This results in a negative charge on the surface of the PTFE and a positive charge on the surface of the water

https://doi.org/10.1021/acsami.4c09044
ACS Appl. Mater. Interfaces 2024, 16, 47050−47074

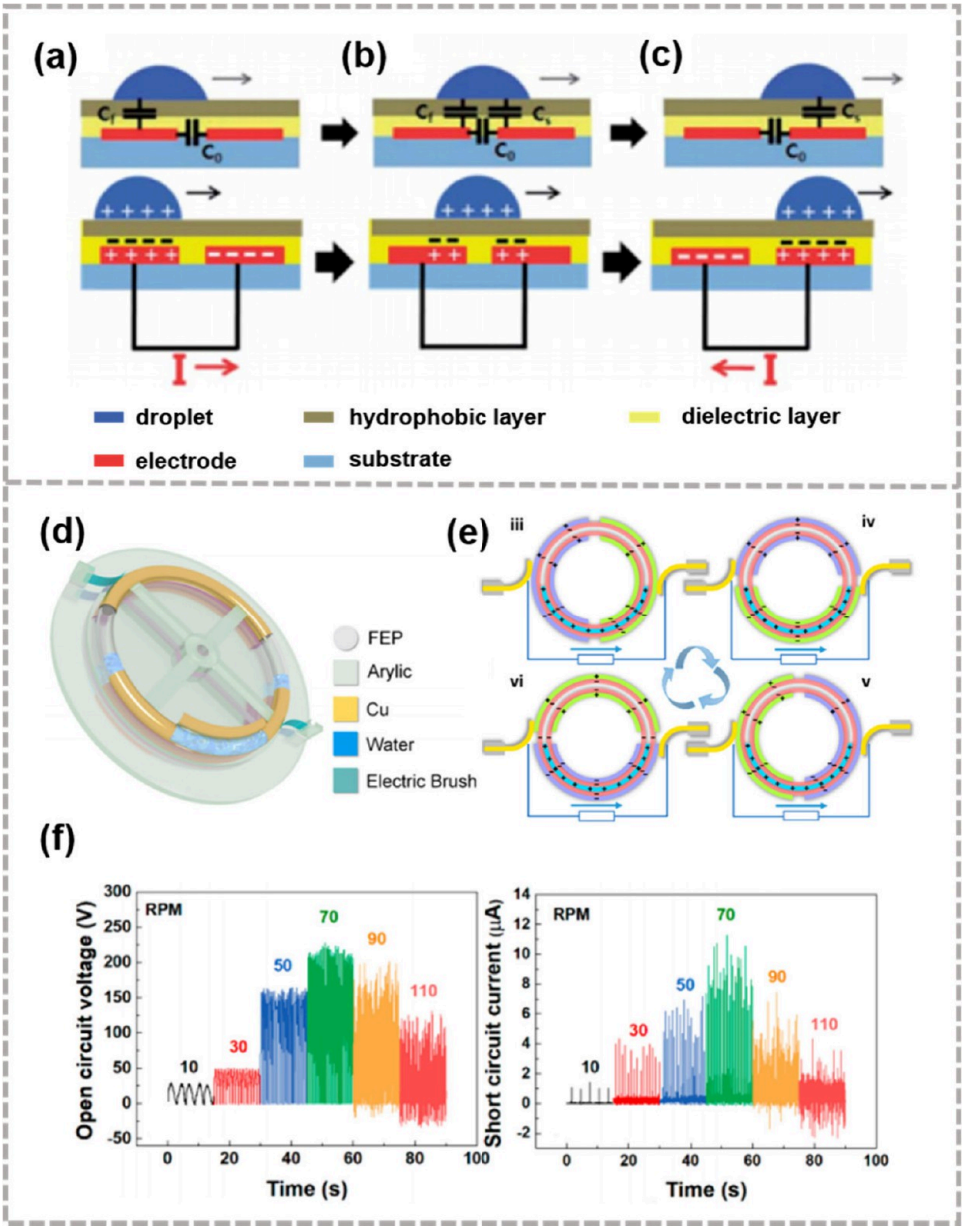

Figure 4. Free-standing mode droplet-based triboelectric nanogenerators. (a−c) The working principle of the free-standing droplet-based nanogenerators. Reproduced with permission from ref 48. Copyright 2014 The Royal Society of Chemistry. (d,e) A DC droplet-based nanogenerator and (f) the open-circuit voltage and short-circuit current of the DC droplet-based nanogenerator. Reproduced with permission from ref 65. Copyright 2019 American Chemical Society.

droplet. EDL is then formed to maintain the electrical neutrality of the system [Figure 3b(ii)]. The area of EDL increases with the increase of droplet diffusion area and reaches the maximum [Figure 3b(iii)]. When the droplet gradually leaves the PTFE film, the electric balance is destroyed, and the electrostatic induction between the PTFE film and the copper electrode establishes the negative potential difference between the copper electrode and the ground. The electron is transferred from the copper electrode to the ground [Figure 3b(iv)] and reaches equilibrium [Figure 3b(v)], which produces an instantaneous negative current. Since the frictional charge on the PTFE film can be retained for a long time, the negative charge on the PTFE surface will attract the counterions in the water droplet to establish a new EDL when the subsequent water droplets fall, resulting in a positive potential difference between the copper electrode and the ground. Electrons flow from the ground to the copper electrode [Figure 3b(vi)] until equilibrium is reached [Figure 3b(vii)]. This process produces an instantaneous positive current. When the water droplet gradually leaves the PTFE surface, a negative potential difference will be established between the copper electrode and the ground, and the electrons will flow from the copper electrode to the ground [Figure 3b(viii)] until a new equilibrium is re-established. This process produces an instantaneous negative current. When the subsequent water droplets periodically contact with the PTFE film, a continuous AC output will be obtained.

When the single-electrode mode droplet-based nanogenerators were first proposed, the peak voltage generated by 30 μL water droplets is 9.3 V, the peak current is 17 μA, and the maximum output power is 145 μW when the load resistance is 5 MΩ.[52] The single- electrode mode has simple structure and

https://doi.org/10.1021/acsami.4c09044
ACS Appl. Mater. Interfaces 2024, 16, 47050−47074

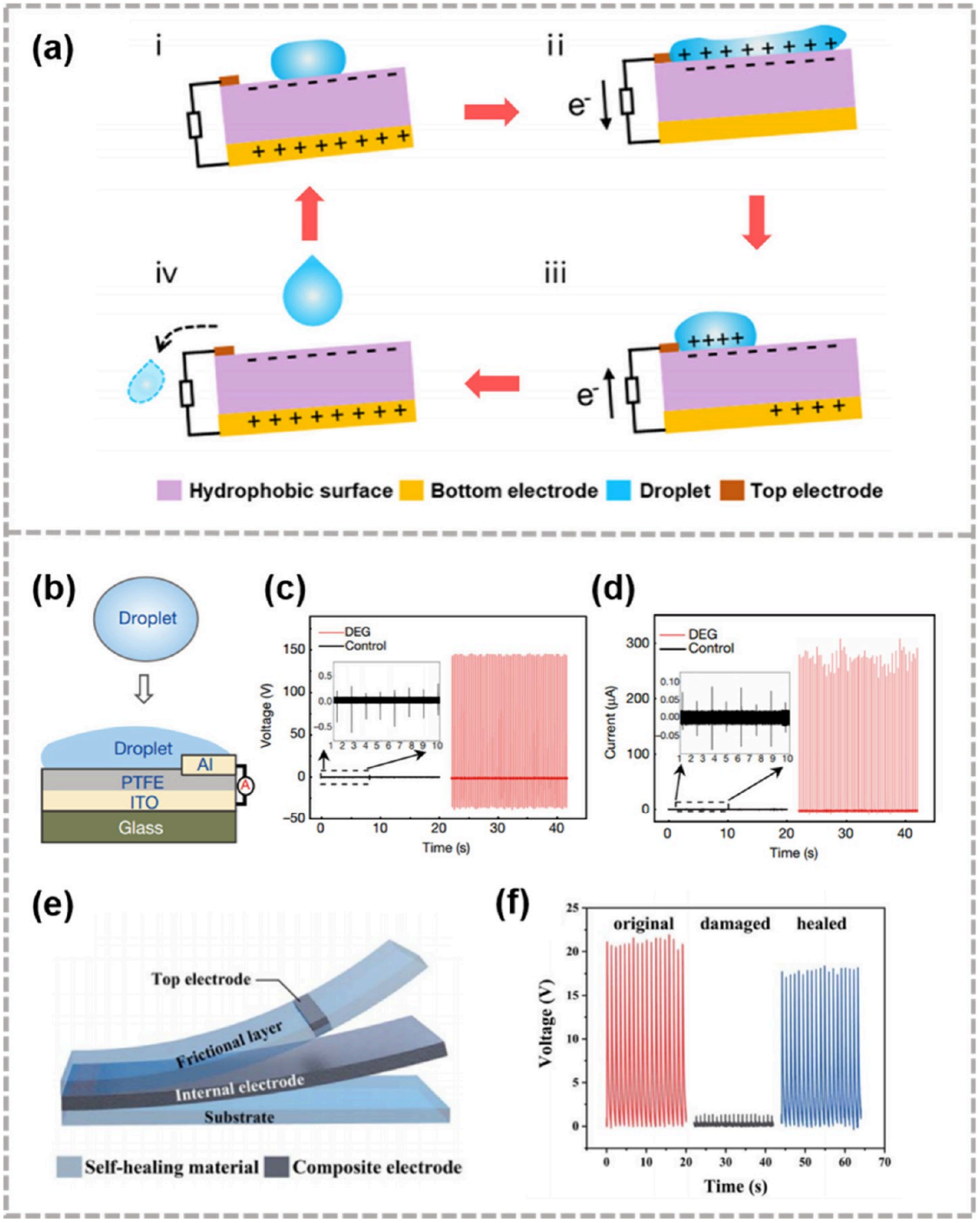

Figure 5. Transistor-inspired mode droplet-based triboelectric nanogenerators. (a) Working principle of the transistor-inspired mode droplet-based nanogenerators. Reproduced with permission from ref 66. Copyright 2021 American Chemical Society. (b−d) Innovatively proposed transistor-inspired mode droplet-based TENG and its output. Reproduced with permission from ref 49. Copyright 2020 Springer. (e,f) A fully self-healing droplet-based nanogenerator. Reproduced with permission from ref 73. Copyright 2022 The Royal Society of Chemistry.

stable performance, but its output performance is limited due to the low induction efficiency caused by the interface effect.[53−55] In Yang et al.'s study, the dynamics of droplets were observed by a high-speed camera, and a robust working mechanism considering the diffusion, rebound, sliding and coalescence of droplets on the solid surface in the triboelectric cycle was proposed, which is significant to guide the subsequent research on droplet-based TENG.[56] Li et al. designed a local bottom electrode to enhance the electrostatic induction through the electrode area and the blank area, so that the peak output voltage can reach up to 30 V.[57] Wang et al. inherited the design of this local electrode and developed an induced electric enhanced droplet-based triboelectric nanogenerator (IED-TENG), as shown in Figure 3c.[58] The device mainly includes a PTFE film as a friction layer and a small-sized copper electrode. Comparing IED-TENG with traditional single-electrode droplet-based triboelectric nanogenerator (D-TENG), it can be seen that D-TENG completely encapsulates the metal electrode with a dielectric layer, the interface effect and electrostatic shielding effect limit the

https://doi.org/10.1021/acsami.4c09044
ACS Appl. Mater. Interfaces 2024, 16, 47050−47074

output performance (Figure 3d,e). However, due to the reduction of the electrode size, the electric field generated by the surface potential difference on both sides of the electrode edge promotes the redistribution of free charges in the droplet diffusion layer and enhances the electrostatic induction effect. By considering the droplet dynamics, optimizing the electrode shape and parameter configuration, a peak output voltage of about 70 V and a peak output current of 6 μA are achieved (Figure 3f,g). The single-electrode mode droplet-based nanogenerators will play a greater role in raindrop energy collection in the future due to its excellent stability and scalability.

3.2. Free-Standing Mode Droplet-Based Nanogenerators. In addition to the single-electrode mode, the free-standing mode droplet-based nanogenerators are also used for droplet energy harvesting.[48,59−61] The working principle of the free-standing mode droplet-based nanogenerators is shown in Figure 4a−c.[48] The device consists of a glass substrate, an indium tin oxide (ITO) electrode, a poly(4-vinylphenol) (PVP) dielectric layer, and an EKG6015N hydrophobic layer. For clarity, the power generation process of the free-standing mode droplet-based nanogenerators is divided into three steps. In the first step, the water droplets are positively charged by contact with the PVP layer, and the PVP layer is negatively charged (Figure 4a). EDL is generated at the interface between the water droplet and the PVP layer, the positive charges accumulate on the first electrode to maintain charge neutrality, and the negative charges move to the second electrode at the same time. In the second step, the water droplets move to the middle of the first and second electrodes (Figure 4b). The overlap area of the water droplet and each electrode is equal, reaching an electrostatic equilibrium state with no charge transfer occurring. In the third step, the water droplets completely cover the second electrode. The positive charge of the water droplet attracts the negative charge of the PVP layer (Figure 4c), causing charge to move from the second electrode to the first electrode. The whole process produces an instantaneous AC output. When the water droplet begins to overlap with the second electrode and no longer overlaps with the first electrode, the output reaches the maximum due to the maximum difference between the overlapping regions. In this free-standing mode, when 30 μL of water droplets slide along a 7 mm-wide electrode, a peak voltage of 3.1 V and a peak current of 5.3 μA can be generated.

Although the free-standing mode droplet-based nanogenerators shows greater potential to increase output than the single-electrode mode, the charge transfer mechanism of droplet evolution in it is still unclear. Zhao et al.'s research results show that for the free-standing mode droplet-based nanogenerators, the output current can be increased to more than 100 times by controlling the size of the droplet impact center relative to the electrode gap.[62] They proposed an asymmetric capacitance-induced charge transfer mechanism, which well explains this current enhancement phenomenon. The free-standing mode droplet-based nanogenerators outputs alternating current, if you want to achieve a self-powered power system, you need an external rectifier or regulator circuit, which will undoubtedly increase manufacturing costs, energy consumption and reduce the flexibility of the device.[63,64] Therefore, it is necessary to develop a power generator that directly generates direct current (DC). As shown in Figure 4d, Wang and his team proposed a DC droplet-based nanogenerator (DC-TENG).[65] The DC-TENG is composed of an ethylene propylene fluoride (FEP) tube and a copper electrode, which is designed as a ring structure. Two brushes are attached on either side of the device, enabling the generation of DC in the free-standing mode. The tube is filled with fluid medium, when the annular tube rotates under external stimulation, the fluid medium can fully contact with the inner wall of the FEP tube, resulting in sufficient contact electrification effect. The working principle is shown in Figure 4e. When the tube is filled with a general volume of deionized (DI) water and the device speed reaches 70 rpm, the peak output voltage and current is as high as 228 V and 11.5 μA (Figure 4f).

3.3. Transistor-Inspired Mode Droplet-Based Nanogenerators. As a significant landmark in the evolution of droplet-based nanogenerators, Xu et al. introduced a transistor-inspired droplet-based electricity generator (DEG) in 2020.[49] The general operating principle of this transistor-inspired mode droplet-based nanogenerator is depicted in Figure 5a.[66] The nanogenerator comprises a top electrode, a friction layer, and a bottom electrode. As droplets continuously land on the hydrophobic surface, the contact electrification effect between the two materials causes the hydrophobic surface to accumulate negative charges until saturation, subsequently entering a stable working cycle. The negative charge on the hydrophobic layer induces an equal magnitude of positive charge on the bottom electrode. A water droplet falling from a height spreads upon the hydrophobic surface, and contact electrification takes place. Prior to the water droplet making contact with the top electrode, all induced charges are situated on the bottom electrode [Figure 5a(i)], resulting in no electrical signal generation. Upon the spreading droplet touching the top electrode, the previously disconnected components form a closed-loop electrical system. Electrons swiftly transfer from the top to the bottom electrode to neutralize the potential difference [Figure 5a(ii)], thereby generating a peak current signal. As the droplet reaches its maximum spread before shrinking and sliding off the hydrophobic surface, the bottom electrode once again induces opposite charges to counterbalance the negative charges on the hydrophobic surface. This induces electron flow from the bottom to the top electrode, generating an inverse peak current [Figure 5a(iii)]. After the droplet completely slides away without contacting the top electrode, the electrical signal vanishes, and the system reverts to its initial equilibrium state, awaiting the arrival of the next droplet to repeat the process and generate a new AC output. Illustrated in Figure 5b, in the transistor-inspired mode droplet-based nanogenerators that first proposed by Xu et al., the generated peak output voltage and current from a single droplet reach approximately 143.5 V (Figure 5c) and 270.0 μA (Figure 5d), which are about 295 and 2600 times higher than those achieved without employing an aluminum top electrode. Additionally, the peak output power achieved is 50.1 W m^{-2}. The PTFE surface, subjected to the continual impact of water droplets, can prestore a high density of charge (49.8 nC). Analogous to the gate-controlled electron flow from source to drain in a field-effect transistor (FET), the DEG device dynamically controls the flow of prestored high-density charges on the PTFE surface between the top and bottom electrodes. This is achieved through the contact-separation dynamics of the droplet and the top electrode, yielding a superior output performance compared to traditional droplet-based nanogenerators.

https://doi.org/10.1021/acsami.4c09044
ACS Appl. Mater. Interfaces 2024, 16, 47050−47074

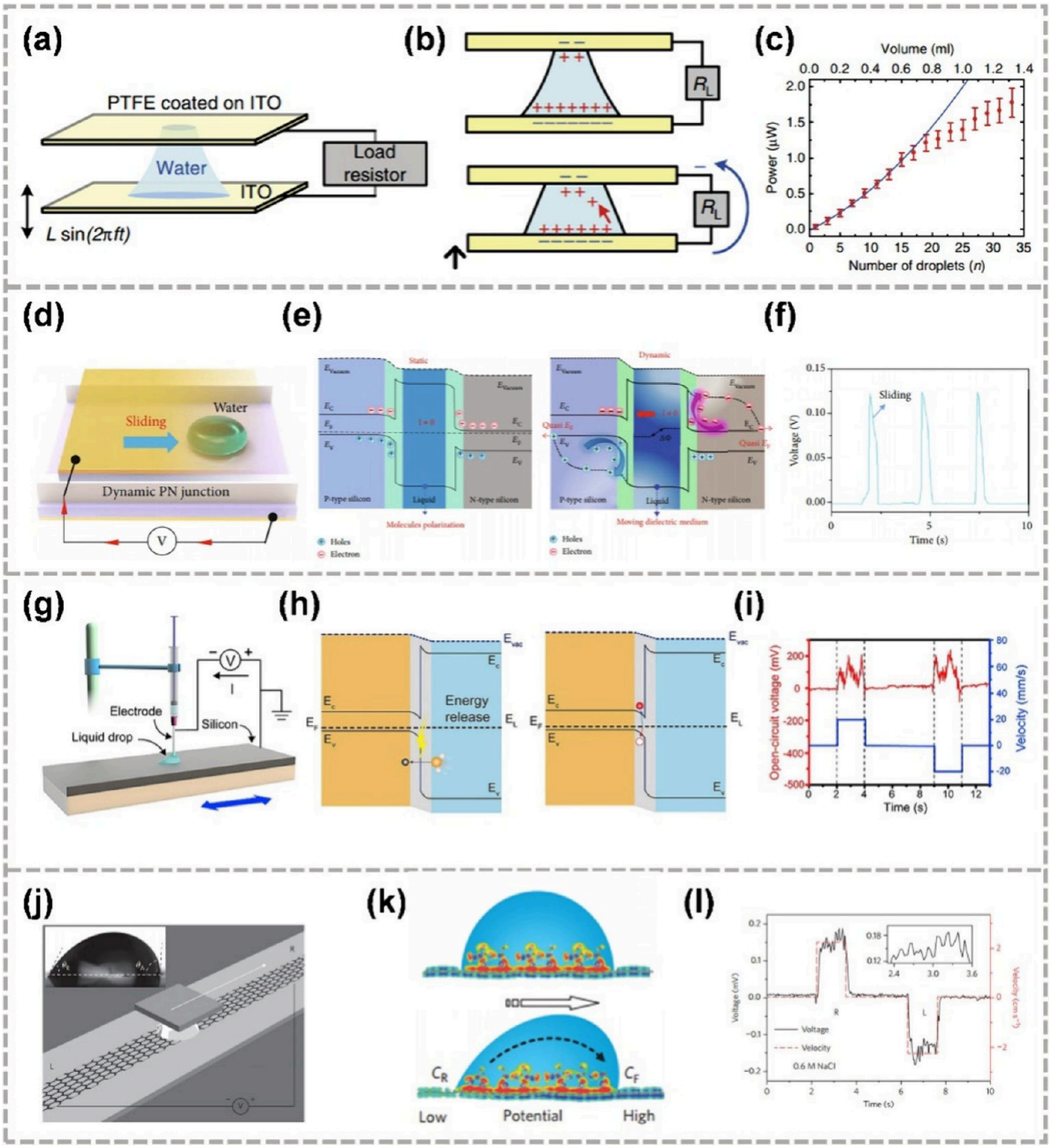

Figure 6. Some other droplet-based nanogenerators in different working modes. (a–c) A power generation device that the interfacial capacitors continuously charge and discharge from each other. Reproduced with permission from ref 77. Copyright 2013 Springer. (d–f) A power generation device using moving liquid droplets sandwiched between different semiconductors. Reproduced with permission under Creative Commons CC BY license from ref 78. Copyright 2021 The Authors. (g–i) A droplet-based nanogenerator based on the tribovoltaic effect. Reproduced with permission from ref 79. Copyright 2020 Elsevier. (j–l) Drawing salt solution droplets on the surface of graphene can generate electricity. Reproduced with permission from ref 80. Copyright 2014 Springer.

Research indicates that the performance of transistor-inspired mode droplet-based nanogenerators is influenced by factors such as electronegativity, hydrophobicity, the thickness of the friction layer, and the dynamics of droplet diffusion.[67−69] Zhang et al. demonstrated that optimal output is achieved when a droplet spreads to its fullest extent at the moment of contacting with the top electrode.[67] However, the energy harvesting process in droplet-based nanogenerators is subject to external mechanical stresses including bending, twisting, and compression. These forces can cause damage to the friction layer and electrodes, thus limiting device output.[70−72] Addressing this challenge, Li and his team developed a fully self-healing droplet-based nanogenerator by incorporating poly(vinylidene fluoride-*co*-hexafluoropropylene) (PVDF-HFP) elastomers with the plasticizer acetyl tributyl citrate (ATBC), as shown in Figure 5e.[73] When the damaged device is immersed in water for 12 h, its output voltage can recover to 85% of its original performance (Figure 5f), with higher temperatures further facilitating the healing process. Such self-healing nanogenerators promise enhanced stability and reliability for practical applications.

https://doi.org/10.1021/acsami.4c09044
ACS Appl. Mater. Interfaces 2024, 16, 47050−47074

3.4. Other Droplet-Based Nanogenerators in Some Different Working Modes. As more and more researchers devote themselves to droplet-based nanogenerators, new droplet-based nanogenerators with unique working modes and principles have gradually been invented.[74] Some research focuses on transistor-inspired droplet-based triboelectric nanogenerators, employing various electrode modifications to enhance performance and offer unique advantages. For example, Li et al. prepared graphene electrodes and reported a droplet-based electricity generator with grounded electrodes, which exhibited good hydrophobicity, corrosion resistance, and stable output performance.[75] In contrast, Yin et al. designed a system where the upper electrode is isolated and does not need to be connected to the lower electrode or ground.[76] Compared to traditional transistor-inspired droplet-based triboelectric nanogenerators, this structure leverages the self-capacitance effect of the upper electrode, achieving an ultrahigh instantaneous power output of up to 765 W m^2.

Additionally, some droplet-based nanogenerators with unique working principles have been proposed. As shown in Figure 6a, a droplet is sandwiched between two ITO electrodes with different hydrophilicity and hydrophobicity, generating an AC voltage by mechanically modulating the electrical double layers at the interface of a water bridge between two conducting plates (Figure 6b).[77] The output voltage arises from electric double-layer capacitors formed at the two interface regions, which continuously charge and discharge each other in different phases, and the output power increases quadratically with the number of droplets (Figure 6c). Lin's research team used a similar structure, sandwiching moving droplets between two semiconductors with different Fermi levels (Figure 6d).[78] The dynamic polarization process of water molecules moving between the semiconductors can continuously output a DC voltage of about 0.12 V (Figure 6e,f). Also using semiconductors, Figure 4g shows a droplet-based nanogenerator based on the tribovoltaic effect.[79] A conductive needle drives a deionized water (DI water) droplet to slide on the surface of a silicon wafer. The built-in electric field generated between the liquid and the semiconductor drives and separates electron−hole pairs, synchronously obtaining a DC signal (Figure 6h,i). In the research by Guo et al., the same method of dragging droplets was used, but NaCl droplets were dragged on a single layer of graphene (Figure 6j).[80] As shown in Figure 6k,l, the generated electrical energy is derived from a novel electrokinetic phenomenon where a pseudocapacitor formed under the droplet is driven forward, charging and discharging at the droplet's boundary.

The above primarily introduces three working modes of droplet-based nanogenerators, as well as some emerging devices with unique working principles for generating electricity using droplets in recent years. When these three modes were first proposed, the single-electrode mode and free-standing mode droplet-based nanogenerators exhibited lower induction efficiency and output voltage compared to the transistor-inspired mode due to interfacial effects. However, in subsequent research, through the design of electrode structures and control of droplet dynamic motion, the output performance of the three modes has reached the same order of magnitude. In the future, the choice of mode will depend more on the application scenarios. The single-electrode mode and free-standing mode droplet-based nanogenerators, due to the electrodes not directly contacting the droplets and having lower requirements for droplet collision dynamics, will have advantages in harvesting water energy in natural environment. The transistor-inspired mode, on the other hand, shows greater potential for significantly improving output performance. Future research should focus more on enhancing the performance of triboelectric materials, such as electronegativity, hydrophobicity, self-healing properties, and environmental friendliness. For emerging devices utilizing droplet energy harvesting, more efforts are needed in principle exploration, performance enhancement, and practical applications.

4. EVAPORATION-INDUCED NANOGENERATORS

The hydrological cycle, characterized by the evaporation, condensation, falling, and flow of water, catalyzes significant energy conversion processes. Among these, the kinetic energy harbored in falling raindrops can be harnessed using droplet-based nanogenerators. Furthermore, evaporation—a critical component of the hydrological cycle—plays a vital role in regulating environmental temperature and humidity. Exploring the energy potential within the water evaporation process is of considerable application importance. In 2017, research initiatives led by Guo and Zhou et al. unveiled electricity generation from water evaporation in nanocarbon materials (Figure 9a).[81] Echoing the principles of traditional streaming potential, the capillary forces sustained by water evaporation propel water through micronano channels, fostering the accumulation of counterions and thereby generating a potential difference. This groundbreaking discovery has since spurred widespread research interest in nanogenerators driven by water evaporation.[82−86] For evaporation-induced nanogenerators, scientists pay more attention to the solid−liquid interface and the properties of nanomaterials. Therefore, this section first takes a closer look at the EDL at the solid−liquid interface and streaming potential based on Section 2.2, which is generally acknowledged as the working principle of evaporation-induced nanogenerators. Subsequently, the latest advancements in evaporation-induced nanogenerators, spanning material classification, device structures, and performance enhancement strategies, are further reviewed.

4.1. Schematic of the EDL and Streaming Potential at Solid−Liquid Interface. According to the hybrid EDL theory described in Section 2.2, when the solution comes into contact with the solid surface, atomic-level contact between the solution molecules and the solid molecules occurs, resulting in electrostatic charges on the solid surface due to electron transition when the electron clouds overlap strongly. After that, the solution molecules are pushed off the solid surface. The counterions in the solution are attracted by the charged solid surface to form EDL due to the Coulomb interaction. The EDL consists of the Stern layer and the diffusion layer. The Stern layer is composed of polar ions (such as cations) tightly adsorbed on the solid surface. Driven by the Coulomb force, the anions of the diffusion layer are adsorbed near the Stern layer, thereby shielding the potential of the Stern layer (Figure 7a).[18] The potential at the shear plane between the Stern layer and the diffusion layer is called Zeta potential. In addition to Zeta potential, Debye length (λ_D) is also an important parameter to describe EDL, which represents the boundary between the shear plane and the closest bulk liquid region. In some studies, λ_D is also considered as a measure of EDL thickness.[37,40,87−89]

The various phenomena caused by external forces applied to a liquid (such as pressure, gravity, electric field force), leading

https://doi.org/10.1021/acsami.4c09044
ACS Appl. Mater. Interfaces 2024, 16, 47050−47074

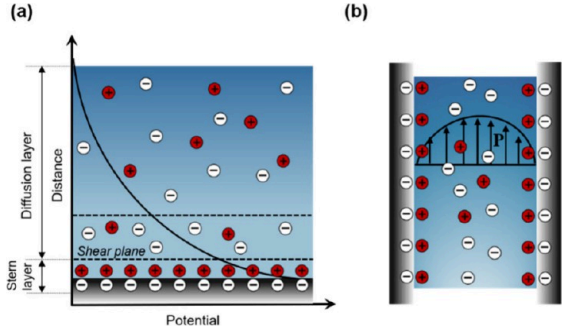

Figure 7. Schematic of the EDL and streaming potential at the liquid−solid interface. (a) EDL consists of Stern layer and diffusion layer and (b) external pressure causes directional flow of counterions in micro/nanochannels. Reproduced with permission under Creative Commons CC BY-NC-ND 4.0 license from ref 18. Copyright 2021 The Authors.

to relative motion between the diffusion layer and the Stern layer, are referred to as the electrokinetic effect.[90] According to the different driving force and motion form, the electrokinetic effect can be divided into electroosmosis, electrophoresis, deposition potential and streaming potential. The streaming potential has a significant advantage in converting waste mechanical energy into electrical energy. When the solution is confined in nanochannels with a size comparable to the λ_D of the solution, the EDL will overlap significantly, resulting in a confined solution dominated by counterions. The fluid motion driven by the pressure gradient ΔP leads to the directional movement of counterions in the diffusion layer and induces a stable electromotive force V_s at both ends and a current I_s flowing through the fluid channel (Figure 6b). The calculation formula of current is

$$I_s = \frac{A\varepsilon_r\varepsilon_0\Delta P\xi}{\eta l} \quad (1)$$

In the formula, l and $A(A = \pi d^2/4)$ are the length and cross-sectional area of the channel in which d is the channel diameter, the potential on the inner surface is ξ, and $\varepsilon_r\varepsilon_0$ and η are the dielectric constant and viscosity of the solution. Therefore, the streaming potential is expressed as

$$V_s = \frac{\varepsilon_r\varepsilon_0\Delta P\xi}{\sigma\eta} \quad (2)$$

where σ denotes the ionic conductivity of the solution and the pressure gradient ΔP is defined as $\Delta P = 4\gamma \cos\theta/d$, where θ is the contact angle between the solution and the channel wall, and γ is the surface tension of the solution. It is evident that the magnitude of streaming potential and streaming current is influenced by factors such as the size and quantity of channels, charge density, and solution properties. The flow energy within nanochannels primarily dissipates due to channel resistance.[91] Consequently, optimizing the channel wall to achieve smoothness represents a strategy to mitigate resistance and enhance flow potential.[92,93]

Streaming potential is the working principle of evaporation-induced nanogenerators recognized by most researchers, but it should be clearly distinguished that streaming potential is different from evaporating potential.[94] The former is the potential generated by driving water through a narrow channel under a pressure gradient, while the latter is caused by the charge transfer in the material directly driven by evaporation of the polar molecules. Furthermore, several theoretical models have been proposed to explain evaporation-induced power generation. These include the ionovoltaic effect, which emphasizes the movement of ions inducing the flow of charge carriers,[95] as well as phonon coupling,[96] Coulombic scattering,[97] and pseudostreaming effect.[98] This paper focus on evaporation-induced nanogenerators induced by streaming potential, which exhibits strong universality.

4.2. Classification of Materials. With the swift progress in materials science, especially with the ongoing emergence of novel nanomaterials, there has been significant development in small-scale power generation devices leveraging these materials. The choice of materials for water evaporation-induced nanogenerators now extends beyond the initial use of carbon-based materials[81,99,100] to encompass biomaterials,[43,82,101] metallic oxide nanomaterials,[102] composite materials,[103−105] among others. This segment outlines the device architecture and efficacy of various functional materials, intending to showcase the progression toward a more diverse material system.

4.2.1. Carbon-Based Materials. Many nanostructure carbon materials exhibit excellent power generation performance under environmental conditions. In 2017, the research team led by Guo and Zhou discovered that the evaporation of centimeter-sized carbon black sheets can reliably generate a continuous voltage of up to 1 V under environmental conditions (Figure 8a), marking the first example of evaporative-induced power generation using cheap carbon black (CB).[81] The SEM image reveals that the prepared CB films are composed of loosely aggregated nanoparticles, with an average diameter of approximately 20 nm (Figure 8b). After annealing and plasma treatment, the CB samples are enriched with abundant functional groups, rendering the samples hydrophilic, thereby ensuring sustained evaporation along the capillary action of the samples. In 2022, the team further demonstrated that the output performance of CB devices is directly generated by the evaporation within the precursor at the forefront of the main capillary.[94] However, the disordered porous structure of carbon materials at the microscopic level can lead to a significant amount of chaotic motion of charge carriers, thereby limiting the improvement of output performance. Inspired by plant xylem vessels, Zhang et al. reported a partially reduced graphene oxide aerogel (prGO) with a regularly arranged porous structure fabricated using an ice templating method, as depicted in Figure 8c.[42] The prGO was obtained through directional freezing of graphene oxide aqueous solution followed by gentle thermal reduction. Facilitated by the directional growth of ice crystals, graphene oxide nanosheets were neatly aligned into a 3D structure featuring ordered channels. The evaporation-based power generation device utilizing this prGO exhibited approximately four times the current of the control sample, demonstrating significant performance enhancement.

4.2.2. Biomaterials. In recent years, biomaterials have garnered increasing interest for their renewable and biodegradable characteristics. A study by Hu et al. showcased an evaporative power generation device employing *Geobacter sulfurreducens* biofilms (Figure 8d).[43] The method involves placing droplets of sulfur-reducing bacteria suspension on a glass slide, allowing them to dry and deposit at room temperature, and then removing the extracellular matrix to form a complete cell biofilm. This approach to device fabrication is both straightforward and cost-effective, enabling

https://doi.org/10.1021/acsami.4c09044
ACS Appl. Mater. Interfaces 2024, 16, 47050−47074

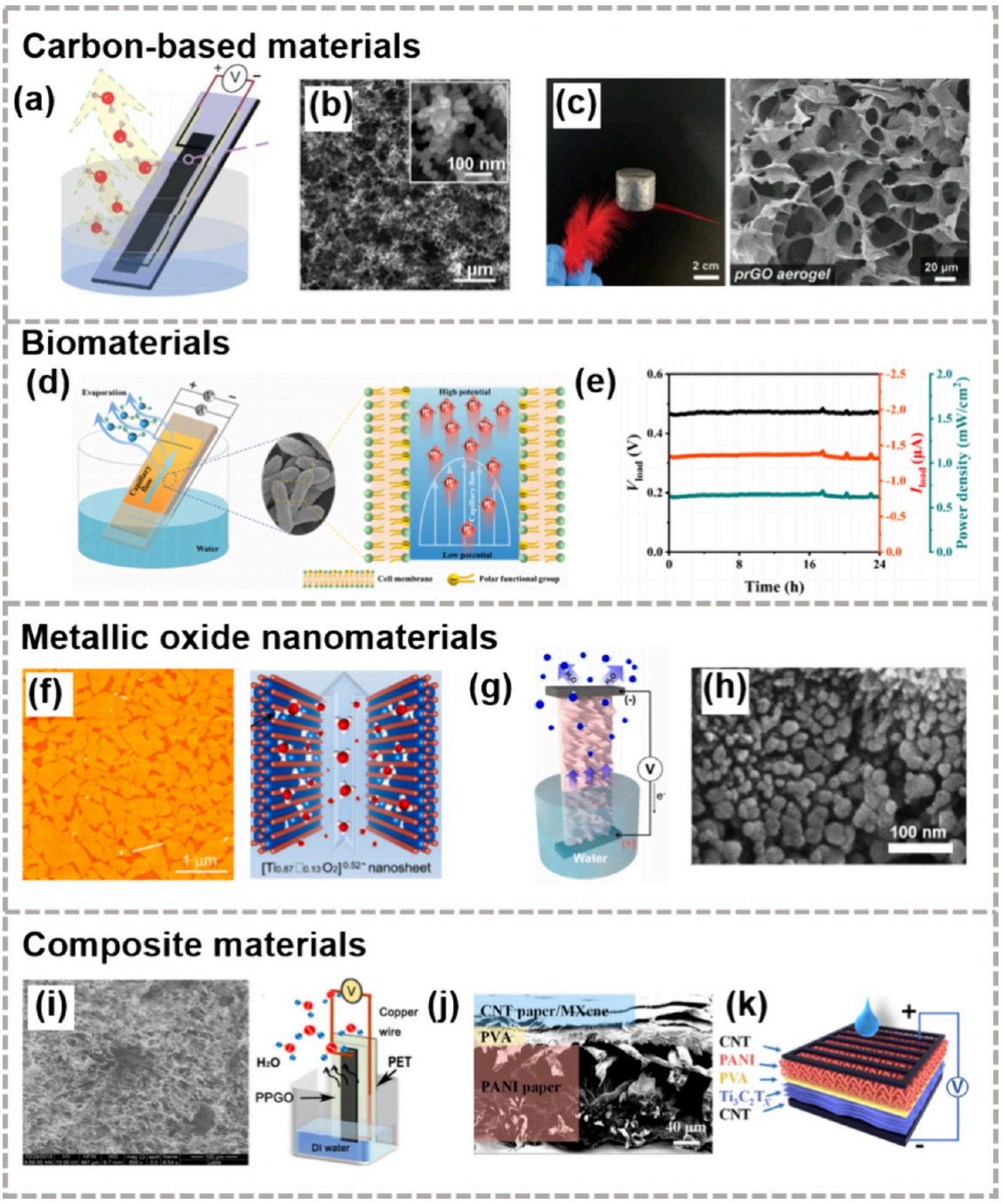

Figure 8. Classification of materials of the water evaporation-induced nanogenerators. (a,b) Power generation device that harvests energy from water evaporation-based carbon black material. Reproduced with permission from ref 81. Copyright 2017 Springer Nature Limited. (c) The evaporation-induced TENG based a partially reduced graphene oxide aerogel and its SEM image. Reproduced with permission from ref 42. Copyright 2023 Wiley-VCH. (d,e) An evaporative power generation device employing *Geobacter sulfurreducens* biofilms and its output. Reproduced with permission under Creative Commons CC BY-NC license from ref 43. Copyright 2022 The Authors. (f) Two-dimensional titanium oxide nanosheets. Reproduced with permission from ref 107. Copyright 2023 Elsevier. (g,h) SEM image of porous ZnO film and schematic diagram of power generation. Reproduced with permission from ref 95. Copyright 2019 American Chemical Society. (i) The device-based PPGO composite aerogel with asymmetric nanostructures. Reproduced with permission from ref 108. Copyright 2020 Elsevier. (j,k) The device-based positively charged conductive polyaniline (PANI) and negatively charged $Ti_3C_2T_x$ MXene. Reproduced with permission from ref 109. Copyright 2021 American Chemical Society.

the generation of continuous electricity. Under optimal conditions, the device has achieved a peak power density of 685.12 μW cm^{-2} (Figure 8e). The power output from devices based on *Geobacter sulfurreducens* biofilms far surpasses that of devices utilizing other materials, attributed to the unique properties of *Geobacter sulfurreducens*. These include its inherent hydrophilicity, water absorption capacity, rich oxygen-containing functional groups, and superior conductivity, all of which enhance water uptake and charge transfer. Additionally, wood offers distinctive advantages used in evaporation-induced nanogenerators with its orderly porous structure and ample polar functional groups. Garemark et al. applied a

https://doi.org/10.1021/acsami.4c09044
ACS Appl. Mater. Interfaces 2024, 16, 47050−47074

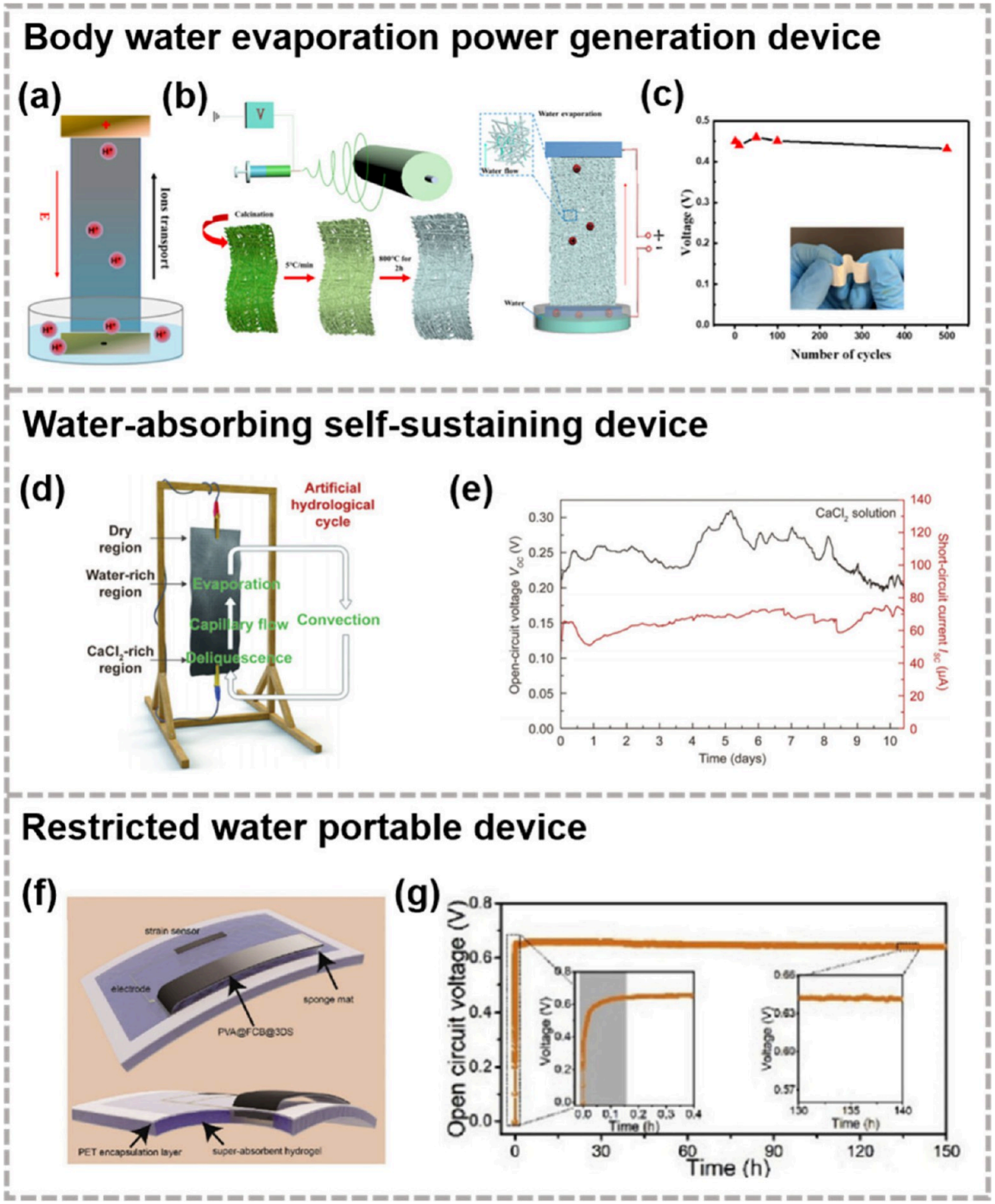

Figure 9. Device structures of water evaporation-induced nanogenerators. (a) The structure of body water evaporation power generation device. (b,c) Ceramic nanofiber-based water-induced electric generator. Reproduced with permission from ref 110. Copyright 2021 American Chemical Society. (d) Water-absorbing self-sustaining device and (e) the output performance. Reproduced with permission from ref 111. Copyright 2020 The Royal Society of Chemistry. (f) Restricted water portable device within highly absorbent hydrogels and (g) its voltage output. Reproduced with permission from ref 112. Copyright 2020 Elsevier.

NaOH treatment to wood to increase its surface area and enable pH-responsive charge dissociation, leading to the development of nanoengineered wood optimized for evaporation-induced power generation.[106] In DI water, this innovative material achieved an open-circuit voltage approximately 140 mV, more than 10-fold the voltage of natural wood. Moreover, by modifying the pH difference between the wood and water, an output voltage of up to 1 V was realized.

4.2.3. Metallic Oxide Nanomaterials. The integration of metallic oxide nanomaterials in hydrovoltaic generators is gaining momentum. In 2023, Zhu's team introduced an innovative approach of atomic-scale Ti vacancy engineering in two-dimensional monolayer titanium oxide nanosheets, aiming

https://doi.org/10.1021/acsami.4c09044
ACS Appl. Mater. Interfaces 2024, 16, 47050−47074

to boost water evaporation-induced power generation, as illustrated in Figure 7f.[107] By strategically designing two-dimensional titanium oxide nanosheets with meticulously controlled Ti atomic vacancy levels, they significantly enhanced the water−solid interaction at the atomic scale. This enhancement facilitated a sustained open-circuit voltage of about 1.32 V for an impressive duration exceeding 250 h. Meanwhile, as depicted in Figure 8g, Kim and colleagues discovered that zinc oxide (ZnO) films, cultivated through solvent-thermal methods, could produce stable and ongoing electricity amid water evaporation processes.[95] The ZnO film has a porous nature with a specific surface area of approximately 57.6 m^2 g^{-1} and pore sizes ranging from ∼5 to ∼200 nm, as shown in Figure 8h. These porous attributes facilitate spontaneous capillary action within the grooves of submicron-scale devices. Within this configuration, when part of the ZnO film dips into DI water, the device can generate an open-circuit voltage around 0.4 V and a short-circuit current approximately 20 nA.

4.2.4. Composite Materials. Composite materials have increasingly been employed in evaporation-induced nanogenerators according to numerous studies. Qi et al. devised a generator utilizing composite aerogels with asymmetric nanostructures, as presented in Figure 8i.[108] This aerogel comprises supramolecular poly(3,4-ethylenedioxythiophene), polystyrenesulfonate, and pyrolyzed polymeric graphene oxide (PPGO). The SEM cross-sectional images reveal that the PPGO composite aerogel possesses a dense nanostructure with uniformly dispersed curved voids. In ambient conditions, water evaporation from a 1.25 cm^2 area of PPGO aerogel is capable of generating a continuous voltage exceeding 0.49 V cm^{-2}. Notably, by leveraging the pyroelectric effect, the device can achieve a maximum voltage of roughly 2.13 V with a temperature difference of 110 K and relative humidity around 73%. This innovation offers a novel approach for water energy harvesting amidst extreme thermal variations. In a similar vein, Li et al. engineered an evaporation-induced nanogenerator with an asymmetric structure, consisting of positively charged conductive polyaniline (PANI) and negatively charged $Ti_3C_2T_X$ MXene.[109] Cross-sectional imagery showcases a three-dimensional micro/nanobraided structure alongside two-dimensional layered channels, augmenting the interaction between water and the active materials (Figure 8j,k). The inclusion of poly(vinyl alcohol) (PVA) between PANI and MXene not only preserves the asymmetric architecture but also enables a peak current density of 1.8 mA cm^{-2}.

4.3. Structures of Devices. The different device structures of evaporation-induced nanogenerators are developed to adapt to different usage environments and fully utilize various forms of water energy. This chapter categorizes device structures into three types: body water evaporation power generation device, water-absorbing self-sustaining device, and restricted water portable device. Representative research works for each type of device structure are introduced accordingly (Figure 9).

Initially, when evaporation-induced nanogenerators emerged, their design primarily leveraged the evaporation of body water for generating electricity.[81] As illustrated in Figure 9a, one end of such a generator is positioned vertically or at an angle into a solution, where the segment exposed to air undergoes continuous wetting due to capillary action, thus ensuring an ongoing evaporation process. Simultaneously, the segment submerged beneath the water surface consistently supplies water, guaranteeing power generation for extended periods. In settings with abundant water sources, this design conceptually supports prolonged energy generation, offering benefits like simplicity and the potential for large-scale energy capture. Nonetheless, the reliance on body water as a power source curtails the broader application of these devices in areas like wearable power sources and biological sensors. Moreover, the durability of the electrode submerged in water warrants careful consideration. Sun et al. utilized sol−gel electrospinning technology to develop an evaporation-induced nanogenerator using SiO_2 nanofibers, as shown in Figure 9b.[110] One end of this device is immersed in deionized water and, even after undergoing 500 bends, it consistently delivered an output of 0.48 V and 0.37 μA, demonstrating no reduction in performance (Figure 9c).

The device designed for water-absorbing self-sustaining evaporation-induced power generation is depicted in Figure 9d.[111] Kim's team ingeniously integrated $CaCl_2$ into the evaporation-induced nanogenerator to create an artificial hydrological cycle, thereby fabricating a self-sustaining water generator (Figure 9d). As illustrated, by applying a $CaCl_2$ solution to one end of the carbon black-coated fabric, the device leverages the hygroscopic nature of $CaCl_2$ to naturally draw moisture from the air, compensating for water dissipated through evaporation. This innovation eliminates the need for repeated manual water replenishment, which is essential for uninterrupted energy harvesting, thereby broadening the applicability of the generator. The device is capable of consistently delivering an electrical output exceeding 0.2 V and 60 μA for over 10 days in conditions of 25 °C and 35% RH, showcasing its capability for prolonged, stable operation (Figure 9e).

Restricted water evaporation-induced power generation forms the third primary device configuration. As demonstrated in Figure 9f, Zhang's team harnessed highly absorbent hydrogels as a water reservoir, creating a sustainable, portable, flexible, and enduring power generation system.[112] Operating under ambient conditions (20.4 °C, 55% RH), the system delivered a steady short-circuit current of 63 μA and an optimized power output of 8.1 μW, maintaining performance for over 150 h (shown in Figure 9g). Furthermore, the generator maintains its efficiency even when subjected to bending deformations of up to 120°, making it an ideal candidate for flexible portable power sources in wearable electronics. Similarly, Saha et al. used hydrophilic agar hydrogel films, enriched with LiCl and glycerol, to replicate natural water cycles.[113] This strategy ensured the continuous operation. The progression from body water evaporation to self-sustained water absorption and then to restricted water portable devices illustrates the evolution of evaporation-induced power generators toward meeting diverse application requirements. Looking ahead, self-sustaining water devices and restricted water evaporation devices are poised for wider adoption, thanks to their versatility, portability, and adaptability. Furthermore, the design of these devices must also address the integrity of the bond between evaporation materials and substrates, alongside considerations such as potential bacterial and dust contamination in the water and the risk of water channel blockages.

4.4. Performance Optimization. The expanding diversity of material choices and the evolution of device structures, propelled by a range of application needs, have introduced new imperatives for enhancing generator performance, with the goal of synergistically elevating power generation efficiency.

https://doi.org/10.1021/acsami.4c09044
ACS Appl. Mater. Interfaces 2024, 16, 47050−47074

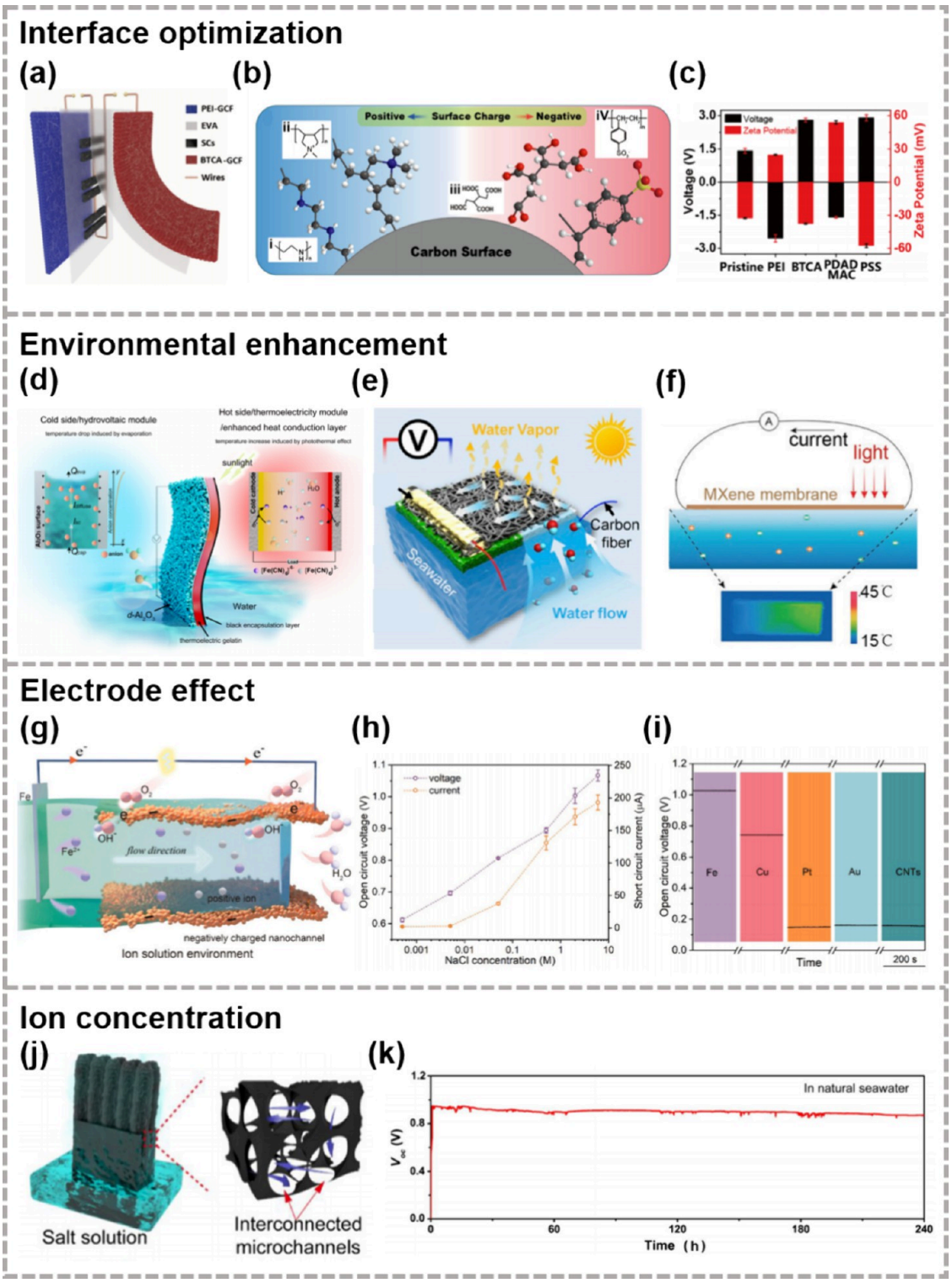

Figure 10. Performance optimization of the water evaporation-induced nanogenerators. (a–c) Asymmetric carbon film generator based on surface modification. Reproduced with permission from ref 116. Copyright 2019 Elsevier. (d) Heat conduction-enhanced evaporation-induced nanogenerator. Reproduced with permission under Creative Commons CC-BY license from ref 119. Copyright 2022 The Author(s). (e) Solar-enhanced evaporation-induced nanogenerator with an asymmetrical build. Reproduced with permission from ref 115. Copyright 2019 Elsevier. (f) Uneven lighting on photothermal MXene films introduces temperature gradients, which drives asymmetrical water evaporation. Reproduced with permission from ref 120. Copyright 2020 Elsevier. (g–i) Evaporation-induced generator that is suitable for high ion concentrations due to Fe electrode reaction. Reproduced with permission from ref 123. Copyright 2021 Elsevier. (j,k) Device that can continuously generate electricity in natural seawater. Reproduced with permission from ref 44. Copyright 2021 American Chemical Society.

Since the inception of evaporation-induced nanogenerators in 2017, a growing array of strategies for performance optimization has emerged prominently.[85,96,97,114,115] In this segment, we examine three principal methods for enhancing

https://doi.org/10.1021/acsami.4c09044
ACS Appl. Mater. Interfaces 2024, 16, 47050–47074

performance: interface optimization, environmental enhancement, and the electrode effect.

4.4.1. Interface Optimization. The text discusses the significance of the porosity, pore size, and channel morphology of functional nanomaterials in influencing the performance of evaporation-induced power generation devices. Moreover, the wettability and Zeta potential of these nanomaterials that related to surface functional groups are pivotal in determining their output efficiency. Consequently, various approaches have been devised to modify the surface functional groups of these materials. These groups are broadly categorized into: (1) intrinsic functional groups, inherent to the nanomaterials, and (2) adjustable functional groups, added through synthetic modification or doping. Figure 10a illustrates a hybrid device featuring two types of glass fiber-carbon nanoparticle films, each tailored with polymers possessing opposite electron affinities.[116] The blue film is treated with a cationic polymer, polyethylenimine (PEI), which imbues it with strong surface positive charges. The amino groups of PEI introduce positive charges on the surface of carbon nanoparticles (CNPs), which are naturally negatively charged, thereby inverting the output voltage from approximately 1 V to −3.2 V. Conversely, the red film is adjusted with 1,2,3,4-butanetetracarboxylic acid (BTCA), rich in carboxyl groups (−COOH), effectuating a voltage increase from about 1.5 V to approximately 3 V (Figure 10b,c). However, an overabundance of cross-linking chains due to high polymer modifier concentrations can obstruct the nanochannels, capping the electrical output of this hybrid apparatus at 5 V and 1.5 μA.

4.4.2. Environmental Enhancement. Substantial research has demonstrated the direct influence of water evaporation rates on the electrical output of evaporation-induced nanogenerators.[44,117,118] These rates significantly depend on environmental factors like temperature, humidity, and wind speed. Annually, the atmosphere, oceans, and landmasses harness approximately 3,850,000 exajoules of solar energy, with a large fraction being absorbed by water molecules as vibration and heat, thereby facilitating the evaporation process. Consequently, to amplify water evaporation rates and thus boost the efficiency of evaporation-driven nanogenerators, initiatives to efficiently merge solar with water energy have been pursued. As Illustrated in Figure 10d, Li et al. crafted a heat conduction-enhanced evaporation-induced nanogenerator by affixing flexible ion thermoelectric (i-TE) gelatin onto the reverse side of porous dual-sized Al_2O_3 (d-Al_2O_3).[119] In this design, the i-TE material bolsters thermal conductivity between the d-Al_2O_3 and its surroundings, elevating the evaporation rate. The d-Al_2O_3 module, through persistent water evaporation, maintains a steady temperature difference of about 2 K for the thermoelectric module. Exposed to standard sunlight, the device consistently delivers an open-circuit voltage of 6.4 V. In another instance, Xiao et al. introduced a solar-enhanced evaporation-induced nanogenerator with an asymmetrical build (Figure 10e),[115] where a double-layer carbon nanotube film/cellulose paper, asymmetrically coated with hydrophobic polydimethylsiloxane (PDMS), propels directional water movement. With sunlight, the open-circuit voltage and short-circuit current elevate from roughly 0.47 V and 15 μA (in absence of light) to approximately 0.6 V and 22 μA, validating the positive impact of sunlight on evaporation rates. Furthermore, uneven lighting on photothermal MXene films introduces temperature gradients, driving asymmetrical water evaporation and enhancing water circulation (Figure 10f), allowing a single device (0.5 cm × 2 cm) to register a short-circuit current of 12 μA.[120]

4.4.3. Electrode Effect. In Section 4.3, it is highlighted that for all body water evaporation devices, and in certain self-sustaining and restricted water evaporation devices, at least one electrode is in direct contact with water. This necessitates an evaluation of potential electrochemical reactions affecting power generation. In 2011, Dhiman et al. demonstrated an instance where approximately 30 mV was generated as a hydrochloric acid solution passed through a graphene film flanked by two metal electrodes submerged in the solution.[121] Yet, Yin et al.'s subsequent 2012 investigation revealed that this voltage generation ceased when the metal electrodes were isolated from the solution, indicating that the electricity stemmed from the direct contact of the electrodes with the solution rather than from the interaction between the solution and the graphene film.[122] Thus, in designing water evaporation-induced nanogenerators, it is essential to discern whether electricity generation arises from the nanomaterial-solution interaction or from chemical reactions at the electrode−solution interface. In a comprehensive 2021 study, Li et al. scrutinized the role of an active metal (Fe) electrode within a composite membrane (dust-free paper, PVA, and carbon black particles) in an evaporation-induced generator.[123] Figure 10g depicts how a primary battery forms between the Fe electrode and the composite membrane in a high ion concentration solution, with the cathodic reaction being $2Fe - 4e^- \rightarrow 2Fe^{2+}$ and the anodic reaction as $O_2 + 4e^- + 2H_2O \rightarrow 4OH^-$. As the NaCl concentration escalates from 0.5 mM to 6 M, the output power surges by two magnitudes (Figure 10h), thanks to the redox reactions enabled by the Fe electrode. In comparison, traditional generators with inert electrodes like Au, Pt, and CNTs muster only a 0.15 V voltage in a 2 M NaCl solution. Conversely, devices with Fe active electrodes can attain an open-circuit voltage of up to 1.04 V (Figure 10i), illustrating how electrode effects can amplify the electrical output in specific scenarios of evaporation-induced nanogenerators. The work of Liu et al. further demonstrated that the output of evaporation-induced nanogenerators with active electrodes can be thousands of times higher than that of devices with inert electrodes.[124] Identifying the presence of electrode effects involves manipulating environmental conditions. The native electrical output of such nanogenerators is markedly sensitive to environmental parameters like wind speed and humidity, in contrast to the output from electrode reactions, which remains largely unaffected by these elements. Yang et al. conducted a comprehensive analysis of the electrode reactions existing in the active electrodes of the evaporation generator using both theoretical and experimental methods, which helps us to gain a deeper understanding and identify them.[125]

4.4.4. Ion Concentration. Moreover, it is essential to recognize that the performance of evaporation-induced nanogenerators is not solely influenced by material interface properties, environmental conditions, and electrode effects but also significantly by the characteristics of the solution itself. Recent research highlights how an increase in the ion concentration of the solution can adversely affect the generated electrical energy.[97,105,126] This adverse effect is attributed to the increase in ion concentration leading to a shorter Debye length, which in turn weakens the overlap of the EDL within micronano channels, diminishing the output performance. Nonetheless, Wu et al. demonstrated in their 2021 study that

https://doi.org/10.1021/acsami.4c09044
ACS Appl. Mater. Interfaces 2024, 16, 47050−47074

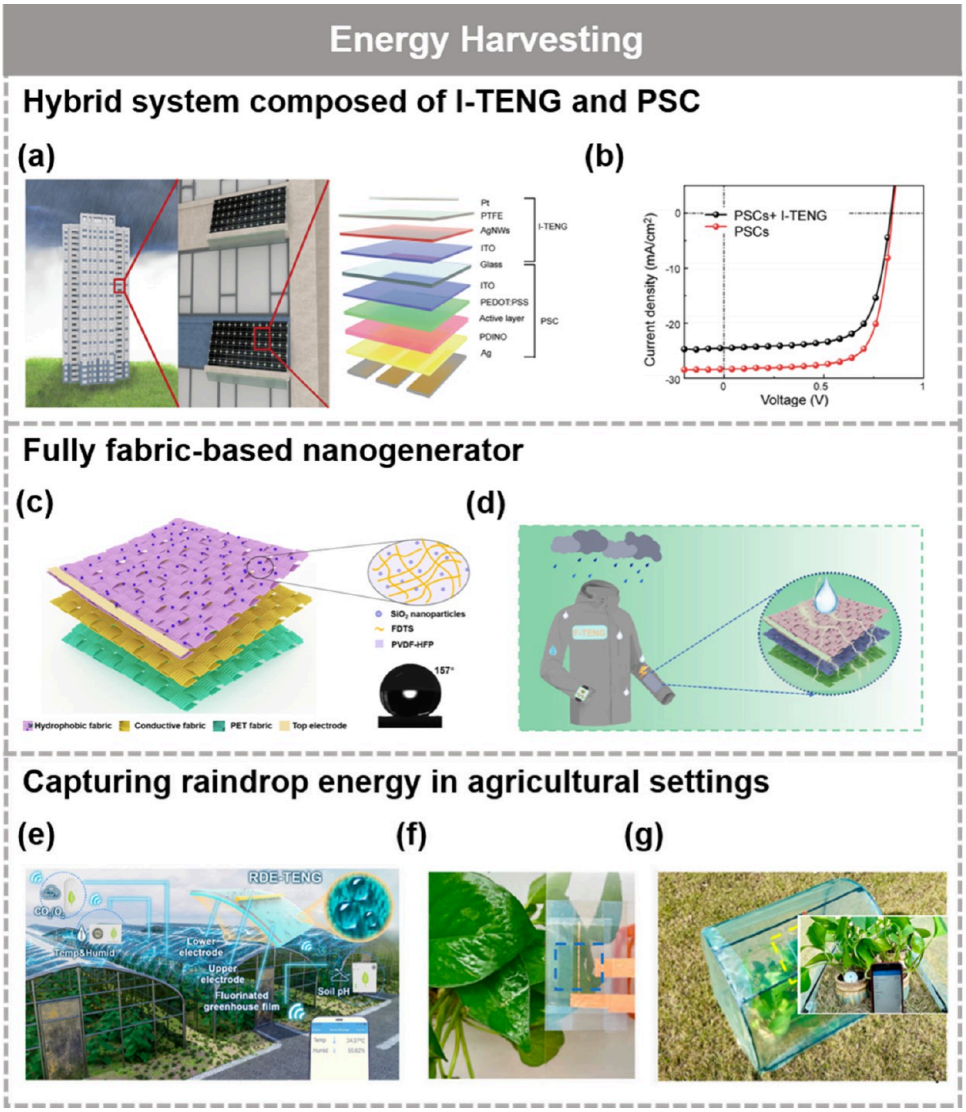

Figure 11. Applications in energy harvesting of liquid−solid triboelectrification-based nanogenerators. (a) Hybrid system composed of I-TENG and PSC. (b) J−V curve of PSCs and PSCs + I-TENG. Reproduced with permission from ref 127. Copyright 2022 Wiley-VCH. (c) A fully fabric-based droplet-based triboelectric nanogenerator and (d) envisioned integrations into smart raincoats. Reproduced with permission from ref 66. Copyright 2021 American Chemical Society. (e−g) The concept for capturing raindrop energy within agricultural settings. Reproduced with permission from ref 131. Copyright 2021 American Chemical Society.

an optimal salt concentration could enhance the output potential and power.[44] The power generator utilized honeycomb-structured reduced graphene oxide films, showcased continuous operation in natural seawater for more than 240 h, underscoring the potential for evaporation-induced nanogenerators in seawater applications (Figure 10j,k). This growing interest in seawater environments for such generators underscores the need for a nuanced understanding of solution characteristics in optimizing device performance.

5. APPLICATIONS OF LIQUID−SOLID TRIBOELECTRIFICATION-BASED NANOGENERATORS

Thanks to the concerted efforts of researchers globally, the past decade has witnessed substantial advancements in liquid−solid triboelectrification-based nanogenerators, paving the way for innovative applications such as energy harvesting and self-powered sensing. Furthermore, the high compatibility of most devices has spurred their emerging use in health care applications. This section offers an in-depth exploration of the diverse applications of liquid−solid triboelectrification-based nanogenerators.

5.1. Applications in Energy Harvesting. Droplet-based nanogenerators have low demands on water sources owing to their unique structures and working principle. Additionally, their design is ideally suited for harvesting energy from natural raindrops, leading to their widespread adoption for this application.

Figure 11a presents a multilayered hybrid energy harvesting system that combines an instantaneous droplet-based nanogenerator (I-TENG) with a perovskite solar cell (PSC), creating a versatile all-weather energy harvester.[127] The innovative stepped array structure of the devices ensures that water droplets from upper layers efficiently fall onto the lower layers, optimizing the utilization of both potential and kinetic energy from each raindrop. Figure 11b depicts the current−voltage curves for both the hybrid I-TENG/PSC device and

https://doi.org/10.1021/acsami.4c09044
ACS Appl. Mater. Interfaces 2024, 16, 47050−47074

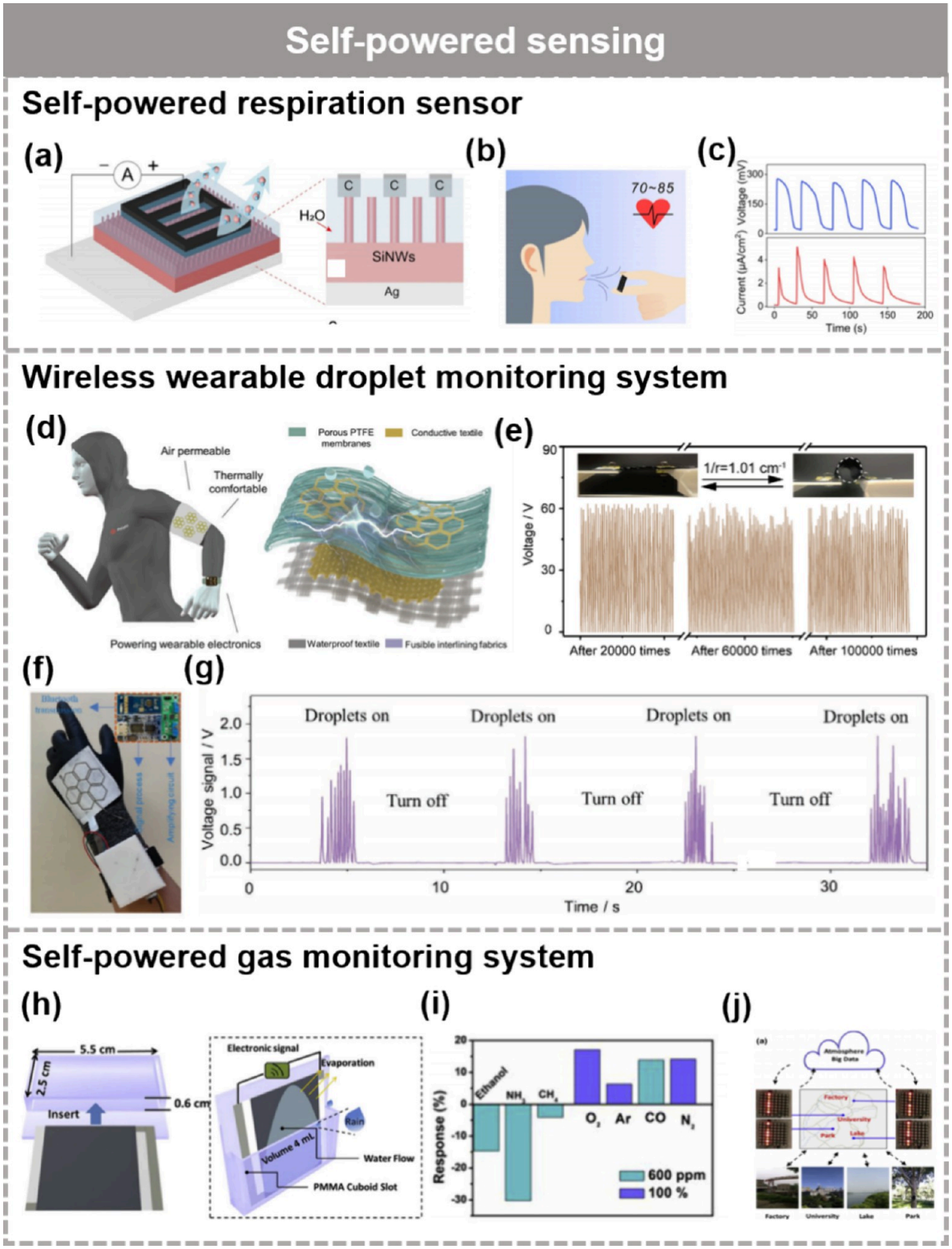

Figure 12. Applications in self-powered sensors of liquid−solid triboelectrification-based nanogenerators. (a) A hydroelectric device utilizing silicon nanowire arrays. (b,c) Self-powered respiration sensor. Reproduced with permission from ref 132. Copyright 2020 Wiley-VCH. (d) Topology-optimized liquid droplet energy harvesting fabrics. (e) Cyclic bending deformation test. (f,g) Wireless wearable droplet monitoring system. Reproduced with permission from ref 133 .Copyright 2021 Wiley-VCH. (h) Self-powered gas monitoring system aimed at establishing comprehensive atmospheric data. (i) Detection of various gases and (j) real-time environmental surveillance and the generation of extensive atmospheric data. Reproduced with permission from ref 134. Copyright 2019 Elsevier.

standalone PSCs under simulated sunlight conditions (AM1.5G, 1000 W cm^{-2}). Although the PSCs showcase a remarkable power conversion efficiency (PCE) reaching up to 17.1%, the hybrid setup still demonstrates a commendable

https://doi.org/10.1021/acsami.4c09044
ACS Appl. Mater. Interfaces 2024, 16, 47050−47074

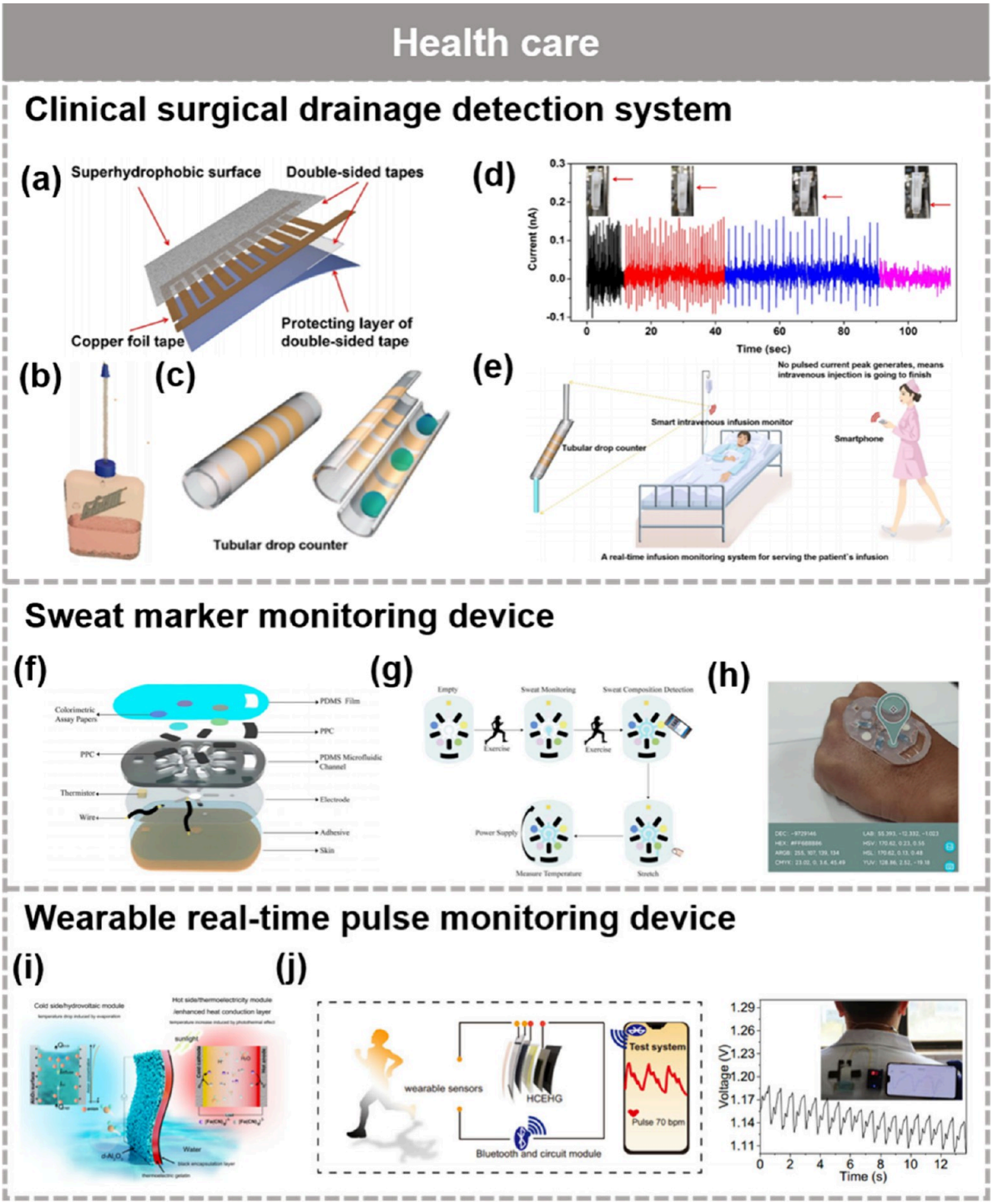

Figure 13. Applications in health care of liquid−solid triboelectrification-based nanogenerators. (a−e) A droplet sensor with superhydrophobic droplet interfaces utilizing silica nanoparticles to monitor drainage activities. Reproduced with permission from ref 135. Copyright 2020 American Chemical Society. (f−h) Electronics skin with monitoring sweat volume and various physiological markers. Reproduced with permission from ref 136. Copyright 2023 The Royal Society of Chemistry. (i) A thermally enhanced evaporation-induced nanogenerator and (j) real-time pulse detection. Reproduced with permission from 119. Copyright 2022 Springer.

PCE of 14.4%. The superhydrophobic surface of TENG also plays a critical role in maintaining the PSC standard conversion efficiency by ensuring a consistently clean surface. However, the limitations of traditional polymer films used in water droplet energy harvesting—such as inadequate breathability, poor skin compatibility, and lack of reparability—severely restrict their potential for wearable technology.[128−130]

Addressing these challenges, Ye et al. introduced a fully fabric-based droplet-based triboelectric nanogenerator (F-TENG).[66] Illustrated in Figure 11c, the friction layer of the F-TENG features a superhydrophobic fabric engineered with SiO_2 nanoparticles and poly(vinylidene fluoride-*co*-hexafluoropropylene) (PVDF-HFP) cografted with perfluorodecyltrichlorosilane (FDTS). This composition not only bestows the

https://doi.org/10.1021/acsami.4c09044
ACS Appl. Mater. Interfaces 2024, 16, 47050−47074

fabric with super hydrophobicity but also imparts thermoplastic elastomer characteristics to the PVDF-HFP, enabling self-healing properties. Envisioned for integration into smart raincoats (Figure 11d), the F-TENG achieves an overall energy conversion efficiency of 2.9%, heralding new possibilities for wearable energy harvesting devices. Establishing a sustainable energy source is crucial for the management of intelligent greenhouse environments. Zhang et al. developed a concept for capturing raindrop energy within agricultural settings (Figure 11e).[131] Through the use of inductively coupled plasma (ICP) etching to alter polyethylene (PE) film, a superhydrophobic surface was crafted, leading to the creation of a completely transparent droplet-based nanogenerator device (Figure 11f). By incorporating this device into greenhouse coverings, it acts as a renewable energy supply for humidity sensors in greenhouses, aiding in the intelligent regulation of agricultural production environments (Figure 11g).

In the future, liquid−solid triboelectrification-based nanogenerators are expected to be more widely used in energy harvesting across multiple fields. Droplet-based nanogenerators, in particular, will be highly suitable for energy collection in natural environments due to their unique principles and structures. Integrating these nanogenerators with mature photovoltaic and photothermal technologies can enhance the energy utilization efficiency of both systems, making them valuable in industries such as smart agriculture, smart transportation, and smart energy. Additionally, they can be incorporated into wearable fabrics to create a new generation of portable energy systems. By continuously improving materials and structures, these technologies will further enhance environmental stability and scalability, driving the development and application of sustainable energy solutions.

5.2. Applications in Self-Powered Sensing. Liquid−solid triboelectrification-based nanogenerators have significantly advanced the development and practical application of self- powered sensors. As shown in Figure 12a, Qin et al. engineered a hydroelectric device utilizing silicon nanowire arrays, achieving over 55 mA of short-circuit current density and 6 μW cm^{-2} of power density.[132] Leveraging its sensitivity to moisture, they constructed a respiration sensor predicated on humidity measurement, showcasing a perfect synchronization between the respiration rate and the output voltage and current frequencies (Figure 12b). During respiration, the sensor could achieve a maximum current density exceeding 3 mA (Figure 12c). A method for attaining the highest stable output through topological optimization of the top electrode was demonstrated, tailored for fabric-based nanogenerators that exhibit remarkable resistance to bending deformation (Figure 12d,e).[133] This optimized design achieved a peak power density of 71.8 mW m^{-2}, substantially outperforming the power output of conventional transistor-inspired mode droplet-based nanogenerators by nearly five times. Expanding on this innovation, a wearable liquid-drop sensing system was crafted for autonomous sensing applications (Figure 12f). Integrated into a wristband, this wearable technology is capable of wirelessly transmitting electrical signals in real-time to a portable computer, enabling immediate detection and frequency analysis of droplets (Figure 12g). Zhong et al. introduced an innovative self-powered gas monitoring system aimed at establishing comprehensive atmospheric data, utilizing a novel water evaporation/gas coupling effect.[134] This system employs a mixed slurry film composed of toluene soot, ethyl cellulose, and turpentine alcohol as its functional materials, adeptly transforming natural energy sources into electrical energy (Figure 12h). The generator demonstrated exceptional gas sensitivity, making it suitable for the detection of various gases such as oxygen, ethanol, and ammonia (Figure 12i). The paramount utility of this self-powered gas monitoring system, energized by rainwater, lies in its capability for real-time environmental surveillance and the generation of extensive atmospheric data (Figure 12j). This system opens up new avenues for monitoring air quality, which has profound implications for both economic productivity and public health.

Liquid−solid triboelectrification-based nanogenerators, with their unique working principles, exhibit excellent sensing performance for water vapor and droplets in the environment. In future research, by enhancing encapsulation techniques, optimizing material stability, designing sensor arrays, and reducing the devices' adverse environmental impacts, liquid−solid triboelectrification-based nanogenerators will see further development in areas such as human sensing, raindrop sensing, and environmental monitoring.

5.3. Applications in Health Care. Because of the diverse material selection, superior compatibility, and wearable nature of liquid−solid triboelectrification-based nanogenerators, their applications in health care have piqued significant interest of late. Known for their ability to repel water and bodily fluids like tissue fluid, blood, and urine, superhydrophobic surfaces can pioneer new frontiers in healthcare device innovation. The research team led by Guang Yang has innovated nanogenerators with superhydrophobic droplet interfaces utilizing silica nanoparticles, as delineated in Figure 13a.[135] Initially, this nanogenerator was ingeniously integrated into a disposable drainage bottle, equipped with a droplet sensor to adeptly monitor drainage activities (Figure 13b). This sensor enables real-time data collection and analysis during drainage procedures, aiding in the precise determination of the operation's conclusion and thus mitigating patient discomfort. Subsequently, the team crafted a smart intravenous infusion detector for clinical oversight of infusion procedures (Figure 13c). Figure 13d demonstrates that the output current of the detector reflects the different positions of the infusion tube's regulating valve. Integrated with wireless signal transmission technology, the real-time infusion monitoring system provides valuable information about infusion operations for nurses and patients (Figure 13e). Sweat analysis emerges as a potential diagnostic tool for identifying disease, monitoring progression, assessing dehydration, and evaluating mental stress levels. Figure 13f illustrates the innovative design of self-powered sweat electronics skin (SE-skin) based on microchannels.[136] This SE-skin comprises four layers; the topmost utilizes PDMS to absorb atmospheric water vapor for moisture electricity generation, while the second layer features PDMS microchannels to harvest sweat for electricity generation through evaporation. Sandwiched between these layers are the evaporation-induced and moisture-induced nanogenerator modules, a thermistor temperature sensor, and a colorimetric paper module, employing grapefruit peel carbon paper (PSS) to facilitate dual nanogenerator functions. The third layer functions as electrodes, with the fourth providing adhesive properties for secure skin attachment. When affixed to the skin, SE-skin can monitor sweat volume and various physiological markers, including chloride ions, uric acid, glucose, lactate, and pH levels (Figure 13g,h). Furthermore, Li et al. introduced a thermally enhanced hydraulic nanogenerator that combines flexible ion thermoelectric and evaporation-induced electricity

https://doi.org/10.1021/acsami.4c09044
ACS Appl. Mater. Interfaces 2024, 16, 47050−47074

Table 1. Summarizing the Recent Droplet-Based Nanogenerators and Evaporation-Induced Nanogenerators with Their Structures, Functional Materials, Device Output, and Applications

nanogenerators types (materials/structure)	structures	functional materials	device outputs	applications	refs
Droplet-based nanogenerators	Single-electrode mode	PTFE	V_{oc} = 70 V I_{sc} = 6 μA	Harvesting droplets' kinetic energy	58
	single-electrode mode	PTFE	V_{oc} = 30 V I_{sc} = 24.3 μA	Harvesting turbulent energy	55
	Free-standing mode	FEVE	V_{oc} = 80 V I_{sc} = 18 μA	Metal Cathodic Protection	60
	Free-standing mode	FEP	V_{oc} = 228 V I_{sc} = 11.5 μA	DC power supply, self-powered chemical sensor	65
	Free-standing mode	Superhydrophobic film with SiO_2 nanoparticles	I_{sc} = 5 nA accumulated charge = 5 nC	Clinical drainage monitoring	135
	Transistor-inspired mode	PTFE	V_{oc} = 143.5 V I_{sc} = 270.0 μA	Harvesting raindrops' energy	49
	Transistor-inspired mode	porous PTFE membrane	peak power density = 71.8 W m^2	Wireless wearable droplet monitoring system	133
	Transistor-inspired mode	SiO_2+PVDF-HFP/FDTS	V_{oc} = 22 V Induced charge = 7.5 nC	Raindrop energy harvesting fabric	66
Evaporation-induced nanogenerators	body water evaporation	All-printed porous carbon film	V_{oc} = 1 V Power density = 8.1 μW cm^{-3}	Electrodeposition of silver microstructures	97
	body water evaporation	SiO_2 nanofiber	V_{oc} = 0.48 V I_{sc} = 0.37 μA	Power supply	110
	body water evaporation	d-Al_2O_3	V_{oc} = 6.4 V	Wearable pulse monitoring	119
	water-absorbing self-sustaining	Carbon-coated cotton fabric	V_{oc} = 0.74 V I_{sc} = 22.5 μA	Power supply	111
	restricted water evaporation	PVA@FCB@3DS	V_{oc} = 0.658 V I_{sc} = 63 μA	Wearable power supply, flexible sensor	112
	restricted water evaporation	Reconstructed V_2O_5 membrane	V_{oc} = 0.56 V I_{sc} = 18 μA	Power supply in low humidity environment	113

generation (Figure 13i).[119] This innovation is capable of driving real-time pulse detection via pressure sensors attached to the radial artery (Figure 13j).

With the progress of society, people's health awareness is gradually increasing, and health care devices are attracting more attention from researchers. Liquid−solid triboelectrification-based nanogenerators can be used in clinical monitoring for infusion and intraoperative drainage monitoring. They can also be developed into self-powered sweat sensors for accurate detection and concentration analysis of sweat biomarkers. Especially for the latter, by improving the sensitivity, flexibility, and wearing comfort of the devices in the future, the application of liquid−solid triboelectrification nanogenerators in monitoring health status through sweat analysis will develop rapidly.

6. CONCLUSION AND PERSPECTIVES

This article delivers an exhaustive overview of water energy harvesting technologies that leverage liquid−solid triboelectrification, encompassing both droplet-based nanogenerators and water evaporation-induced nanogenerators. Initially, we delve into the liquid−solid contact electrification mechanism guided by Wang's transition model, alongside the formation of the EDL at the solid−liquid interface illuminated by Wang's hybrid model. The discourse progresses to the architectural and functional nuances of droplet-based nanogenerators, which are systematically classified into single-electrode, free-standing, and transistor-inspired modalities. After that, the forefront of research in the materials, device structures and performance optimization of water evaporation-induced nanogenerators are reviewed. Culminating the review, we highlight the representative applications of liquid−solid triboelectrification-based nanogenerators in the realms of energy harvesting, self-powered sensing and health care.

In Table 1, we summarize and compare the recent research progress on droplet-based nanogenerators and water evaporation-induced nanogenerators. It can be seen that there are obvious differences in structure between the two liquid−solid triboelectrification-based nanogenerators. Droplet-based nanogenerators can be divided into three categories according to their working principles, while evaporation-induced nanogenerators have the same fundamental principles and can only be categorized based on their application scenarios. Although the fundamental principal models of the two nanogenerators are liquid−solid triboelectrification, their working mechanisms differ, leading to significant differences in their functional materials and device outputs. The functional materials of droplet-based nanogenerators are mainly polymers with strong electronegativity, such as PTFE and FEP. However, the functional materials of evaporation-based nanogenerators are carbon-based materials, biomaterials, metal oxides, and other materials with rich micronano structures and abundant functional groups. The former's device output voltage is much higher than that of the latter, but it is an AC output. The latter has a slightly larger current and provides a sustainable DC output. In terms of applications, droplet-based nano-

https://doi.org/10.1021/acsami.4c09044
ACS Appl. Mater. Interfaces 2024, 16, 47050−47074

generators are clearly more suitable for harvesting energy from natural raindrops, while evaporation-induced nanogenerators can be further adapted for use in wearable power sources or sensors.

However, despite the extensive progress summarized in this article, the practical application of liquid−solid triboelectrification-based water energy harvesting technologies still faces several critical challenges that urgently need to be addressed:

(1) For water evaporation-induced nanogenerators, their working mechanism remains somewhat unclear. The current models proposed are still phenomenological and lack more advanced in situ characterization techniques to reveal the underlying charge generation and transfer processes. Various explanations currently proposed, including streaming potential, ionovoltaic effect, and pseudostreaming effect are likely to occur simultaneously in a system and require further elucidation of the thermo-electro-kinetic synergistic effects on the entire system. Additionally, particular attention should be paid to chemical reactions that may occur at the liquid−solid interface, which could interfere with mechanistic studies. Furthermore, the conversion of ion flow at the electrode into electron flow also requires further exploration.

(2) The synthesis of materials and optimization of their properties require more standardized design principles. For the frictional layers of droplet-based nanogenerators, new materials should be developed considering factors such as wettability, surface polarity, and charge density. Regarding water evaporation-induced nanogenerators, developing nanomaterials with specific properties (such as pore size, porosity, wettability, zeta potential, and conductivity) in a more standardized manner would be advantageous to meet various requirements in practical applications.

(3) Further enhancements in conversion efficiency and output power are essential. Despite notable advancements in the efficiency and power output of water-energy harvesting technologies utilizing liquid−solid frictional electrification, their performance largely remains at the microscale. It is crucial to refine device architectures, enhance interfacial properties, advance integration methodologies, and boost overall device output to align with the requisites of practical applications.

(4) The bulk of present advancements and experimental studies are confined to laboratory settings, revealing a substantial disparity from practical applicability. The rigorous conditions encountered in actual environments, such as elevated temperatures, intense humidity, and robust winds, impose stringent requirements on the encapsulation and durability of materials used in devices. Moreover, the transition to practical applications demands attention to scalability, cost-effectiveness, and eco-friendliness, factors critical for mass production and widespread adoption.

In summary, liquid−solid triboelectrification-based hydropower harvesting technology has witnessed remarkable advancements in recent years. This method offers a cleaner alternative to conventional fossil fuel-based power generation, with the ability to transform low-grade water energy from the environment into high-quality electrical power. This is vital for reducing energy constraints and promoting the achievement of carbon neutrality objectives. With continued dedication, we have the unprecedented opportunities to devise novel approaches for overcoming the significant hurdles associated with liquid−solid triboelectrification technology (Figure 14).

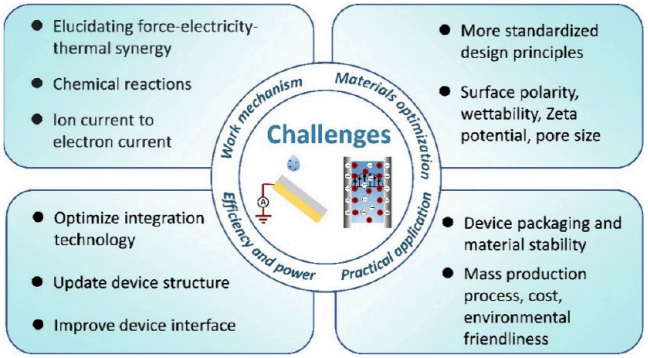

Figure 14. Conclusion and perspectives of liquid−solid triboelectrification-based nanogenerators. Reproduced with permission under Creative Commons CC BY-NC-ND 4.0 license from ref 18. Copyright 2021 The Authors.

AUTHOR INFORMATION

Corresponding Authors

Yang Zou − *Beijing Institute of Nanoenergy and Nanosystems, Chinese Academy of Sciences, Beijing 101400, China; School of Medical Technology, Beijing Institute of Technology, Beijing 100081, China*; Email: zouyang@bit.edu.cn

Zhou Li − *Beijing Institute of Nanoenergy and Nanosystems, Chinese Academy of Sciences, Beijing 101400, China; School of Nanoscience and Engineering, University of Chinese Academy of Sciences, Beijing 100049, China*; orcid.org/0000-0002-9952-7296; Email: zli@binn.cas.cn

Author

Peng Cheng − *Beijing Institute of Nanoenergy and Nanosystems, Chinese Academy of Sciences, Beijing 101400, China; School of Nanoscience and Engineering, University of Chinese Academy of Sciences, Beijing 100049, China*

Complete contact information is available at: https://pubs.acs.org/10.1021/acsami.4c09044

Notes

The authors declare no competing financial interest.

ACKNOWLEDGMENTS

This study was supported by the National Key Research and Development Program of China (2021YFB3201204), the National Natural Science Foundation of China (T2125003, 82202075), Beijing Natural Science Foundation (L212010), the National Postdoctoral Program for Innovative Talent (BX20220380), China Postdoctoral Science Foundation (2022M710389), and the Fundamental Research Funds for the Central Universities.

REFERENCES

(1) Yang, D.; Yang, Y.; Xia, J. Hydrological cycle and water resources in a changing world: A review. *Geography and Sustainability* **2021**, *2* (2), 115−122.

(2) Ellabban, O.; Abu-Rub, H.; Blaabjerg, F. Renewable energy resources: Current status, future prospects and their enabling

technology. *Renewable and Sustainable Energy Reviews* **2014**, *39*, 748−764.
(3) Mishchuk, N. O. Prospects for Electricity Production by the Reverse Electrodialysis Method. *Journal of Water Chemistry and Technology* **2023**, *45* (1), 18−29.
(4) Guo, Z.-Y.; Cui, W.-Z.; Ji, Z.-Y.; Tumba, K.; Wang, J.; Fu, L.-J.; Zhang, Z.-X.; Liu, J.; Zhao, Y.-Y.; Zhang, Z.-D.; et al. Deep utilization of salinity gradient energy between concentrated seawater and river water by multi-stage reverse electrodialysis. *Desalination* **2023**, *566*, 116900.
(5) Chae, S.; Kim, H.; Gi Hong, J.; Jang, J.; Higa, M.; Pishnamazi, M.; Choi, J.-Y.; Chandula Walgama, R.; Bae, C.; Kim, I. S.; et al. Clean power generation from salinity gradient using reverse electrodialysis technologies: Recent advances, bottlenecks, and future direction. *Chemical Engineering Journal* **2023**, *452*, 139482.
(6) Wang, H.; Sun, Y.; He, T.; Huang, Y.; Cheng, H.; Li, C.; Xie, D.; Yang, P.; Zhang, Y.; Qu, L. Bilayer of polyelectrolyte films for spontaneous power generation in air up to an integrated 1,000 V output. *Nat. Nanotechnol* **2021**, *16* (7), 811−819.
(7) Liu, X.; Gao, H.; Ward, J. E.; Liu, X.; Yin, B.; Fu, T.; Chen, J.; Lovley, D. R.; Yao, J. Power generation from ambient humidity using protein nanowires. *Nature* **2020**, *578* (7796), 550−554.
(8) Zhao, K.; Lee, J. W.; Yu, Z. G.; Jiang, W.; Oh, J. W.; Kim, G.; Han, H.; Kim, Y.; Lee, K.; Lee, S.; et al. Humidity-Tolerant Moisture-Driven Energy Generator with MXene Aerogel-Organohydrogel Bilayer. *ACS Nano* **2023**, *17* (6), 5472−5485.
(9) Fan, F.-R.; Tian, Z.-Q.; Lin Wang, Z. Flexible triboelectric generator. *Nano Energy* **2012**, *1* (2), 328−334.
(10) Li, C.; Luo, R.; Bai, Y.; Shao, J.; Ji, J.; Wang, E.; Li, Z.; Meng, H.; Li, Z. Molecular Doped Biodegradable Triboelectric Nanogenerator with Optimal Output Performance. *Adv. Funct. Mater.* **2024**, *34*, 2400277.
(11) Liu, Z.; Hu, Y.; Qu, X.; Liu, Y.; Cheng, S.; Zhang, Z.; Shan, Y.; Luo, R.; Weng, S.; Li, H.; et al. A self-powered intracardiac pacemaker in swine model. *Nat. Commun.* **2024**, *15* (1), 507.
(12) Luo, R.; Shi, B.; Luo, D.; Li, Z. Self-powered electrical stimulation assisted skin wound therapy. *Sci. Bull.* **2023**, *68*, 1740.
(13) Bai, N.; Xue, Y.; Chen, S.; Shi, L.; Shi, J.; Zhang, Y.; Hou, X.; Cheng, Y.; Huang, K.; Wang, W. A robotic sensory system with high spatiotemporal resolution for texture recognition. *Nat. Commun.* **2023**, *14* (1), 7121.
(14) Xu, C.; Wang, A. C.; Zou, H.; Zhang, B.; Zhang, C.; Zi, Y.; Pan, L.; Wang, P.; Feng, P.; Lin, Z.; et al. Raising the Working Temperature of a Triboelectric Nanogenerator by Quenching Down Electron Thermionic Emission in Contact-Electrification. *Adv. Mater.* **2018**, *30* (38), e1803968.
(15) Zhang, J.; Lyu, B.; Nie, D.; Yu, H.; Tao, K.; Li, Y.; Fu, Y.; Miao, J.; Chang, H.; Yuan, W. High-Efficiency Raindrops Energy Harvester Using Interdigital Electrode. In *2021 IEEE 34th International Conference on Micro Electro Mechanical Systems (MEMS)*, 2021; pp 724−727.
(16) Wang, Z. L.; Wang, A. C. On the origin of contact-electrification. *Mater. Today* **2019**, *30*, 34−51.
(17) Wang, X.; Lin, F.; Wang, X.; Fang, S.; Tan, J.; Chu, W.; Rong, R.; Yin, J.; Zhang, Z.; Liu, Y.; et al. Hydrovoltaic technology: from mechanism to applications. *Chem. Soc. Rev.* **2022**, *51* (12), 4902−4927.
(18) Sun, Z.; Wen, X.; Wang, L.; Ji, D.; Qin, X.; Yu, J.; Ramakrishna, S. Emerging design principles, materials, and applications for moisture-enabled electric generation. *eScience* **2022**, *2* (1), 32−46.
(19) Dao, V.-D.; Vu, N. H.; Thi Dang, H.-L.; Yun, S. Recent advances and challenges for water evaporation-induced electricity toward applications. *Nano Energy* **2021**, *85*, 105979.
(20) Hasan, M. A. M.; Zhang, T.; Wu, H.; Yang, Y. Water Droplet-Based Nanogenerators. *Adv. Energy Mater.* **2022**, *12* (37), 2201383.
(21) Wu, X.; Li, X.; Ping, J.; Ying, Y. Recent advances in water-driven triboelectric nanogenerators based on hydrophobic interfaces. *Nano Energy* **2021**, *90*, 106592.
(22) Wang, L.; Zhang, W.; Deng, Y. Advances and Challenges for Hydrovoltaic Intelligence. *ACS Nano* **2023**, *17* (15), 14229−14252.
(23) Xu, C.; Zi, Y.; Wang, A. C.; Zou, H.; Dai, Y.; He, X.; Wang, P.; Wang, Y. C.; Feng, P.; Li, D.; et al. On the Electron-Transfer Mechanism in the Contact-Electrification Effect. *Adv. Mater.* **2018**, *30* (15), e1706790.
(24) Liu, C-y.; Bard, A. J. Electrons on dielectrics and contact electrification. *Chem. Phys. Lett.* **2009**, *480* (4−6), 145−156.
(25) Lin, S.; Xu, C.; Xu, L.; Wang, Z. L. The Overlapped Electron-Cloud Model for Electron Transfer in Contact Electrification. *Adv. Funct. Mater.* **2020**, *30* (11), 1909724.
(26) McCarty, L. S.; Whitesides, G. M. Electrostatic charging due to separation of ions at interfaces: contact electrification of ionic electrets. *Angew. Chem., Int. Ed. Engl.* **2008**, *47* (12), 2188−2207.
(27) Xia, X.; Wang, H.; Guo, H.; Xu, C.; Zi, Y. On the material-dependent charge transfer mechanism of the contact electrification. *Nano Energy* **2020**, *78*, 105343.
(28) Verners, O.; Lapčinskis, L.; Sherrell, P. C.; Šutka, A. Contact Electrification at Dielectric Polymer Interfaces: On Bond Scission, Material Transfer, and Electron Transfer. *Advanced Materials Interfaces* **2023**, *10* (36), 2300562.
(29) Wang, Z. L. Triboelectric Nanogenerator (TENG)—Sparking an Energy and Sensor Revolution. *Adv. Energy Mater.* **2020**, *10* (17), 2000137.
(30) Wu, C.; Wang, A. C.; Ding, W.; Guo, H.; Wang, Z. L. Triboelectric Nanogenerator: A Foundation of the Energy for the New Era. *Adv. Energy Mater.* **2019**, *9* (1), 1802906.
(31) Sun, M.; Li, Z.; Yang, C.; Lv, Y.; Yuan, L.; Shang, C.; Liang, S.; Guo, B.; Liu, Y.; Li, Z. Nanogenerator-based devices for biomedical applications. *Nano Energy* **2021**, *89*, 106461.
(32) Li, D.; Xu, C.; Liao, Y.; Cai, W.; Zhu, Y.; Wang, Z. L. Interface inter-atomic electron-transition induced photon emission in contact-electrification. *Science Advances* **2021**, *7* (39), abj0349.
(33) Lin, S.; Xu, L.; Chi Wang, A.; Wang, Z. L. Quantifying electron-transfer in liquid-solid contact electrification and the formation of electric double-layer. *Nat. Commun.* **2020**, *11* (1), 399.
(34) Lin, S.; Xu, L.; Xu, C.; Chen, X.; Wang, A. C.; Zhang, B.; Lin, P.; Yang, Y.; Zhao, H.; Wang, Z. L. Electron Transfer in Nanoscale Contact Electrification: Effect of Temperature in the Metal-Dielectric Case. *Adv. Mater.* **2019**, *31* (17), e1808197.
(35) Hou, Y.; Dong, X.; Tang, W.; Li, D. Electron Transfer in Contact Electrification under Different Atmospheres Packaged inside TENG. *Materials* **2023**, *16* (14), 4970.
(36) Qin, H.; Xu, L.; Zhan, F.; Wang, Z. L. Electron transfer induced contact-electrification at oil and oleophobic dielectric interface. *Nano Energy* **2023**, *116*, 108762.
(37) Wu, J. Understanding the Electric Double-Layer Structure, Capacitance, and Charging Dynamics. *Chem. Rev.* **2022**, *122* (12), 10821−10859.
(38) Khademi, M.; Barz, D. P. J. Structure of the Electrical Double Layer Revisited: Electrode Capacitance in Aqueous Solutions. *Langmuir* **2020**, *36* (16), 4250−4260.
(39) Shin, S. J.; Kim, D. H.; Bae, G.; Ringe, S.; Choi, H.; Lim, H. K.; Choi, C. H.; Kim, H. On the importance of the electric double layer structure in aqueous electrocatalysis. *Nat. Commun.* **2022**, *13* (1), 174.
(40) Ringe, S.; Morales-Guio, C. G.; Chen, L. D.; Fields, M.; Jaramillo, T. F.; Hahn, C.; Chan, K. Double layer charging driven carbon dioxide adsorption limits the rate of electrochemical carbon dioxide reduction on Gold. *Nat. Commun.* **2020**, *11* (1), 33.
(41) Huang, C.; Zhao, X.; Liu, S.; Hao, Y.; Tang, Q.; Hu, A.; Liu, Z.; Chen, X. Stabilizing Zinc Anodes by Regulating the Electrical Double Layer with Saccharin Anions. *Adv. Mater.* **2021**, *33* (38), e2100445.
(42) Zhang, J.; Cui, P.; Wang, J.; Ge, Y.; Meng, H.; Feng, C.; Liu, H.; Cheng, G.; Du, Z. Biomimetic Aerogel with Aligned Porous Structures from Ice Templating for Water Evaporation-Induced Electricity Generation. *Adv. Mater. Technol.* **2023**, *8* (18), 2300370.

https://doi.org/10.1021/acsami.4c09044
ACS Appl. Mater. Interfaces 2024, 16, 47050−47074

(43) Hu, Q.; Ma, Y.; Ren, G.; Zhang, B.; Zhou, S. Water evaporation−induced electricity with *Geobacter sulfurreducens* biofilms. *Sci. Adv.* **2022**, *8* (15), abm8047.
(44) Wu, M.; Peng, M.; Liang, Z.; Liu, Y.; Zhao, B.; Li, D.; Wang, Y.; Zhang, J.; Sun, Y.; Jiang, L. Printed Honeycomb-Structured Reduced Graphene Oxide Film for Efficient and Continuous Evaporation-Driven Electricity Generation from Salt Solution. *ACS Appl. Mater. Interfaces* **2021**, *13* (23), 26989−26997.
(45) Li, S. M.; Qiu, Y.; Xie, Y. M.; Wang, X. T.; Wang, K.; Cheng, H.; Zhang, D.; Zheng, Q. N.; Wang, Y. H.; Li, J. F. Synergistic Effects of TiO(2) and Carbon Black for Water Evaporation-Induced Electricity Generation. *ACS Appl. Mater. Interfaces* **2024**, *16* (19), 24863−24870.
(46) Wang, Z.; Huang, Y.; Zhang, T.; Xu, K.; Liu, X.; Zhang, A.; Xu, Y.; Zhou, X.; Dai, J.; Jiang, Z. Unipolar Solution Flow in Calcium-Organic Frameworks for Seawater-Evaporation-Induced Electricity Generation. *J. Am. Chem. Soc.* **2024**, *146*, 1690.
(47) Wang, L.; Li, Y.; Gan, Y.; Zhao, L.; Qin, W.; Ding, L. Rainfall erosivity index for monitoring global soil erosion. *Catena* **2024**, *234*, 107593.
(48) Kwon, S.-H.; Park, J.; Kim, W. K.; Yang, Y.; Lee, E.; Han, C. J.; Park, S. Y.; Lee, J.; Kim, Y. S. An effective energy harvesting method from a natural water motion active transducer. *Energy Environ. Sci.* **2014**, *7* (10), 3279−3283.
(49) Xu, W.; Zheng, H.; Liu, Y.; Zhou, X.; Zhang, C.; Song, Y.; Deng, X.; Leung, M.; Yang, Z.; Xu, R. X.; et al. A droplet-based electricity generator with high instantaneous power density. *Nature* **2020**, *578* (7795), 392−396.
(50) Pan, C.; Meng, J.; Jia, L.; Pu, X. Droplet-Based Direct-Current Electricity Generation Induced by Dynamic Electric Double Layers. *ACS Appl. Mater. Interfaces* **2024**, *16* (14), 17649−17656.
(51) Li, J.; Zhang, Y.; Gao, X.; Mao, Y.; Hu, C.; Long, K.; Sun, C.; Guo, S. Self-Powered Droplet Sensor Based on Triboelectric Nanogenerator toward the Internet-of-Things (IoT) Alarm System. *ACS Applied Electronic Materials* **2023**, *5* (11), 6026−6036.
(52) Lin, Z. H.; Cheng, G.; Lee, S.; Pradel, K. C.; Wang, Z. L. Harvesting Water Drop Energy by a Sequential Contact-Electrification and Electrostatic-Induction Process. *Adv. Mater.* **2014**, *26* (27), 4690−4696.
(53) Li, X.; Ning, X.; Li, L.; Wang, X.; Li, B.; Li, J.; Yin, J.; Guo, W. Performance and power management of droplets-based electricity generators. *Nano Energy* **2022**, *92*, 106705.
(54) Wang, H. L.; Zhang, B.; Chen, T.; Mao, W.; Wang, Y. High-Efficiency Single-Droplet Energy Harvester for Self-Sustainable Environmental Intelligent Networks. *Adv. Energy Mater.* **2023**, *13* (45), 2302858.
(55) Zhang, N.; Gu, H.; Lu, K.; Ye, S.; Xu, W.; Zheng, H.; Song, Y.; Liu, C.; Jiao, J.; Wang, Z. A universal single electrode droplet-based electricity generator (SE-DEG) for water kinetic energy harvesting. *Nano Energy* **2021**, *82*, 105735.
(56) Yang, L.; Wang, Y.; Guo, Y.; Zhang, W.; Zhao, Z. Robust Working Mechanism of Water Droplet-Driven Triboelectric Nanogenerator: Triboelectric Output versus Dynamic Motion of Water Droplet. *Adv. Mater. Interfaces* **2019**, *6* (24), 1901547.
(57) Li, L.; Li, X.; Yu, X.; Shen, C.; Wang, X.; Li, B.; Li, J.; Wang, L.; Yin, J.; Guo, W. Boosting the output of bottom-electrode droplets energy harvester by a branched electrode. *Nano Energy* **2022**, *95*, 107024.
(58) Wang, W.; Zhang, L.; Wang, H.; Zhao, Y.; Cheng, J.; Meng, J.; Wang, D.; Liu, Y. High-Output Single-Electrode Droplet Triboelectric Nanogenerator Based on Asymmetrical Distribution Electrostatic Induction Enhancement. *Small* **2023**, *19* (37), e2301568.
(59) Li, Z.; Cao, B.; Zhang, Z.; Wang, L.; Wang, Z. L. Rational TENG arrays as a panel for harvesting large-scale raindrop energy. *iEnergy* **2023**, *2* (2), 93−99.
(60) Peng, J.; Zhang, L.; Sun, W.; Liu, Y.; Yang, D.; Feng, M.; Feng, Y.; Wang, D. High-efficiency droplet triboelectric nanogenerators based on arc-surface and organic coating material for self-powered anti-corrosion. *Applied Materials Today* **2022**, *29*, 101564.
(61) Chen, G.; Liu, X.; Li, S.; Dong, M.; Jiang, D. A droplet energy harvesting and actuation system for self-powered digital microfluidics. *Lab Chip* **2018**, *18* (7), 1026−1034.
(62) Zhao, Z.; Li, H.; Li, A.; Liu, L.; Xue, L.; Cai, Z.; Yuan, R.; Yu, X.; Song, Y. Two-orders of magnitude enhanced droplet energy harvesting via asymmetrical droplet-electrodes coupling. *Nano Energy* **2023**, *108*, 108213.
(63) Zi, Y.; Guo, H.; Wen, Z.; Yeh, M. H.; Hu, C.; Wang, Z. L. Harvesting Low-Frequency (<5 Hz) Irregular Mechanical Energy: A Possible Killer Application of Triboelectric Nanogenerator. *ACS Nano* **2016**, *10* (4), 4797−4805.
(64) Yang, Y.; Zhang, H.; Wang, Z. L. Direct-Current Triboelectric Generator. *Adv. Funct. Mater.* **2014**, *24* (24), 3745−3750.
(65) Wang, J.; Wu, Z.; Pan, L.; Gao, R.; Zhang, B.; Yang, L.; Guo, H.; Liao, R.; Wang, Z. L. Direct-Current Rotary-Tubular Triboelectric Nanogenerators Based on Liquid-Dielectrics Contact for Sustainable Energy Harvesting and Chemical Composition Analysis. *ACS Nano* **2019**, *13* (2), 2587−2598.
(66) Ye, C.; Liu, D.; Peng, X.; Jiang, Y.; Cheng, R.; Ning, C.; Sheng, F.; Zhang, Y.; Dong, K.; Wang, Z. L. A Hydrophobic Self-Repairing Power Textile for Effective Water Droplet Energy Harvesting. *ACS Nano* **2021**, *15* (11), 18172−18181.
(67) Zhang, Q.; Li, Y.; Cai, H.; Yao, M.; Zhang, H.; Guo, L.; Lv, Z.; Li, M.; Lu, X.; Ren, C.; et al. A Single-Droplet Electricity Generator Achieves an Ultrahigh Output Over 100 V Without Pre-Charging. *Adv. Mater.* **2021**, *33* (51), e2105761.
(68) Zhang, N.; Zhang, H.; Liu, Z.; Xu, W.; Zheng, H.; Song, Y.; Wang, Z.; Zhou, X. Performance transition in droplet-based electricity generator with optimized top electrode arrangements. *Nano Energy* **2023**, *106*, 108111.
(69) Wang, X.; Fang, S.; Tan, J.; Hu, T.; Chu, W.; Yin, J.; Zhou, J.; Guo, W. Dynamics for droplet-based electricity generators. *Nano Energy* **2021**, *80*, 105558.
(70) Lai, Y. C.; Wu, H. M.; Lin, H. C.; Chang, C. L.; Chou, H. H.; Hsiao, Y. C.; Wu, Y. C. Entirely, Intrinsically, and Autonomously Self-Healable, Highly Transparent, and Superstretchable Triboelectric Nanogenerator for Personal Power Sources and Self-Powered Electronic Skins. *Adv. Funct. Mater.* **2019**, *29* (40), 1904626.
(71) Sun, W.; Luo, N.; Liu, Y.; Li, H.; Wang, D. A New Self-Healing Triboelectric Nanogenerator Based on Polyurethane Coating and Its Application for Self-Powered Cathodic Protection. *ACS Appl. Mater. Interfaces* **2022**, *14* (8), 10498−10507.
(72) Dai, X.; Huang, L.-B.; Du, Y.; Han, J.; Zheng, Q.; Kong, J.; Hao, J. Flexible, and Tailorable Triboelectric Nanogenerators for Self-Powered Sensors based on Thermal Effect of Infrared Radiation. *Adv. Funct. Mater.* **2020**, *30* (16), 1910723.
(73) Wang, N.; Zhang, L.; Liu, J.; Li, C. An integrally underwater self-healable droplet-based triboelectric nanogenerator. *J. Mater. Chem. A* **2022**, *10* (38), 20509−20516.
(74) Lin, Z.; Yang, Z. Water droplet energy harvesting. *Droplet* **2024**, *3* (1), e97.
(75) Yang, L.; Yu, J.; Guo, Y.; Chen, S.; Tan, K.; Li, S. An Electrode-Grounded Droplet-Based Electricity Generator (EG-DEG) for Liquid Motion Monitoring. *Adv. Funct. Mater.* **2023**, *33* (36), 2302147.
(76) Li, Z.; Yang, D.; Zhang, Z.; Lin, S.; Cao, B.; Wang, L.; Wang, Z. L.; Yin, F. A droplet-based electricity generator for large-scale raindrop energy harvesting. *Nano Energy* **2022**, *100*, 107443.
(77) Moon, J. K.; Jeong, J.; Lee, D.; Pak, H. K. Electrical power generation by mechanically modulating electrical double layers. *Nat. Commun.* **2013**, *4*, 1487.
(78) Lu, Y.; Yan, Y.; Yu, X.; Zhou, X.; Feng, S.; Xu, C.; Zheng, H.; Yang, Z.; Li, L.; Liu, K.; et al. Polarized Water Driven Dynamic PN Junction-Based Direct-Current Generator. *Research* **2021**, *2021*, 7505638.
(79) Lin, S.; Chen, X.; Wang, Z. L. The tribovoltaic effect and electron transfer at a liquid-semiconductor interface. *Nano Energy* **2020**, *76*, 105070.

(80) Yin, J.; Li, X.; Yu, J.; Zhang, Z.; Zhou, J.; Guo, W. Generating electricity by moving a droplet of ionic liquid along graphene. *Nat. Nanotechnol.* **2014**, *9* (5), 378−383.
(81) Xue, G.; Xu, Y.; Ding, T.; Li, J.; Yin, J.; Fei, W.; Cao, Y.; Yu, J.; Yuan, L.; Gong, L.; et al. Water-evaporation-induced electricity with nanostructured carbon materials. *Nat. Nanotechnol* **2017**, *12* (4), 317−321.
(82) Lin, J.; Zhang, Z.; Lin, X.; Cai, X.; Fu, S.; Fang, X.; Ding, Y.; Wang, X.; Sèbe, G.; Zhou, G. All Wood-Based Water Evaporation-Induced Electricity Generator. *Adv. Funct. Mater.* **2024**, *34* (30), 2314231.
(83) Xu, S.; Zhao, Y.; Jiao, S.; Wang, Z.; Yu, Z.; Sun, C.; Liu, X. Microalgae Film-Derived Water Evaporation-Induced Electricity Generator with Negative Carbon Emission. *Adv. Sci.* **2024**, *11*, e2400856.
(84) Liu, Z.; Liu, C.; Ni, A.; Mao, K.; Chen, L.; Xue, L.; Sun, J.; Wang, X.; Xiong, P.; Zhu, J. Tortuosity regulation of two-dimensional nanofluidic films for water evaporation-induced electricity generation. *Nano Res.* **2024**, *17*, 6192.
(85) Wang, F.; Zhang, Y.; Shi, J.; Sun, L.; Ullah, A.; Zhu, C.; Kim, I. S. Bioinspired and Biodegradable Functionalized Graphene Oxide/Deacetylated Cellulose Acetate Composite Janus Membranes for Water Evaporation-Induced Electricity Generation. *ACS Sustainable Chem. Eng.* **2023**, *11* (26), 9792−9803.
(86) Liu, H.; Cui, P.; Zhang, J.; Wang, J.; Ge, Y.; Zhou, Z.; Meng, Y.; Huang, Z.; Yang, K.; Du, Z.; et al. Harnessing Natural Evaporation for Electricity Generation using MOF-Based Nanochannels. *Small* **2024**, e2400961.
(87) Vacic, A.; Criscione, J. M.; Rajan, N. K.; Stern, E.; Fahmy, T. M.; Reed, M. A. Determination of molecular configuration by debye length modulation. *J. Am. Chem. Soc.* **2011**, *133* (35), 13886−13889.
(88) Gu, P.; Yang, S.; Liu, X.; Yang, G. Development of a simple, molecular dynamics-based method to estimate the thickness of electrical double layers. *Soil Science Society of America Journal* **2020**, *84* (2), 494−501.
(89) Hatsuki, R.; Yujiro, F.; Yamamoto, T. Direct measurement of electric double layer in a nanochannel by electrical impedance spectroscopy. *Microfluid. Nanofluid.* **2013**, *14* (6), 983−988.
(90) Wall, S. The history of electrokinetic phenomena. *Curr. Opin. Colloid Interface Sci.* **2010**, *15* (3), 119−124.
(91) Chang, C.-C.; Yang, R.-J. Electrokinetic energy conversion in micrometer-length nanofluidic channels. *Microfluid. Nanofluid.* **2010**, *9* (2−3), 225−241.
(92) Holt, J. K.; Park, H. G.; Wang, Y.; Stadermann, M.; Artyukhin, A. B.; Grigoropoulos, C. P.; Noy, A.; Bakajin, O. Fast Mass Transport Through Sub−2-Nanometer Carbon Nanotubes. *Science* **2006**, *312* (5776), 1034−1037.
(93) Zhao, C.; Yang, C. Advances in electrokinetics and their applications in micro/nano fluidics. *Microfluid. Nanofluid.* **2012**, *13* (2), 179−203.
(94) Fang, S.; Li, J.; Xu, Y.; Shen, C.; Guo, W. Evaporating potential. *Joule* **2022**, *6* (3), 690−701.
(95) Yoon, S. G.; Yang, Y.; Yoo, J.; Jin, H.; Lee, W. H.; Park, J.; Kim, Y. S. Natural Evaporation-Driven Ionovoltaic Electricity Generation. *ACS Applied Electronic Materials* **2019**, *1* (9), 1746−1751.
(96) Zhang, G.; Duan, Z.; Qi, X.; Xu, Y.; Li, L.; Ma, W.; Zhang, H.; Liu, C.; Yao, W. Harvesting environment energy from water-evaporation over free-standing graphene oxide sponges. *Carbon* **2019**, *148*, 1−8.
(97) Ding, T.; Liu, K.; Li, J.; Xue, G.; Chen, Q.; Huang, L.; Hu, B.; Zhou, J. All-Printed Porous Carbon Film for Electricity Generation from Evaporation-Driven Water Flow. *Adv. Funct. Mater.* **2017**, *27* (22), 1700551.
(98) Ge, C.; Xu, D.; Song, Y.; Liu, Y.; Feng, X.; Gao, C.; Chen, Z.; Liu, K.; Sun, Z.; Fang, J. Fibrous Solar Evaporator with Tunable Water Flow for Efficient, Self-Operating, and Sustainable Hydro-electricity Generation. *Adv. Funct. Mater.* **2024**, 2403608.
(99) Wu, Y.; Huang, H.; Zhou, W.; You, C.; Ye, H.; Chen, J.; Zang, S.; Yun, J.; Chen, X.; Wang, L.; et al. High-Porosity Lamellar Films Prepared by a Multistage Assembly Strategy for Efficient Photothermal Water Evaporation and Power Generation. *ACS Appl. Mater. Interfaces* **2022**, *14* (25), 29099−29110.
(100) Wu, M.; Liang, Z.; Peng, M.; Zhao, B.; Li, D.; Zhang, J.; Sun, Y.; Jiang, L. High evaporation rate and electrical conductivity synergistically boosting porous rGO/CNT Film for water evaporation-driven electricity generation. *Nano Energy* **2023**, *116*, 108771.
(101) Piao, X.; Zhang, P.; Shen, J.; Jin, C.; Wang, J.; Wang, Z. Water-evaporation induced electricity generation inspired by natural tree transpiration. *Sustainable Materials and Technologies* **2024**, *39*, e00836.
(102) Chi, J.; Liu, C.; Che, L.; Li, D.; Fan, K.; Li, Q.; Yang, W.; Dong, L.; Wang, G.; Wang, Z. L. Harvesting Water-Evaporation-Induced Electricity Based on Liquid-Solid Triboelectric Nanogenerator. *Adv. Sci.* **2022**, *9* (17), e2201586.
(103) Liu, T.; Zheng, Y.; Hao, C.; Hong, W.; Wang, F.; Jiang, H.; Hu, Y.; Li, C. Rational design of oriented glass fibers within nanoporous SiO2 films to improve evaporation-induced hydroelectric generation. *Applied Materials Today* **2023**, *32*, 101801.
(104) Tian, J.; Zang, Y.; Sun, J.; Qu, J.; Gao, F.; Liang, G. Surface charge density-dependent performance of Ni−Al layered double hydroxide-based flexible self-powered generators driven by natural water evaporation. *Nano Energy* **2020**, *70*, 104502.
(105) Fang, S.; Chu, W.; Tan, J.; Guo, W. The mechanism for solar irradiation enhanced evaporation and electricity generation. *Nano Energy* **2022**, *101*, 107605.
(106) Garemark, J.; Ram, F.; Liu, L.; Sapouna, I.; Cortes Ruiz, M. F.; Larsson, P. T.; Li, Y. Advancing Hydrovoltaic Energy Harvesting from Wood through Cell Wall Nanoengineering. *Adv. Funct. Mater.* **2023**, *33* (4), 2208933.
(107) Liu, C.; Ye, C.; Wu, Y.; Liu, Y.; Liu, Z.; Chen, Z.; Ma, R.; Sakai, N.; Xue, L.; Sun, J. Atomic-scale engineering of cation vacancies in two-dimensional unilamellar metal oxide nanosheets for electricity generation from water evaporation. *Nano Energy* **2023**, *110*, 108348.
(108) Qi, X.; Miao, T.; Chi, C.; Zhang, G.; Zhang, C.; Du, Y.; An, M.; Ma, W.-G.; Zhang, X. Ultralight PEDOT:PSS/graphene oxide composite aerogel sponges for electric power harvesting from thermal fluctuations and moist environment. *Nano Energy* **2020**, *77*, 105096.
(109) Li, Y.; Wu, Y.; Shao, B.; Song, Z.; Wang, Y.; Qiao, J.; Di, J.; Wei, W.; Song, T.; Sun, B. Asymmetric Charged Conductive Porous Films for Electricity Generation from Water Droplets via Capillary Infiltrating. *Acs Appl. Mater. Inter* **2021**, *13* (15), 17902−17909.
(110) Sun, Z.; Feng, L.; Wen, X.; Wang, L.; Qin, X.; Yu, J. Ceramic Nanofiber-Based Water-Induced Electric Generator. *ACS Appl. Mater. Interfaces* **2021**, *13* (47), 56226−56232.
(111) Bae, J.; Yun, T. G.; Suh, B. L.; Kim, J.; Kim, I.-D. Self-operating transpiration-driven electrokinetic power generator with an artificial hydrological cycle. *Energy Environ. Sci.* **2020**, *13* (2), 527−534.
(112) Li, L.; Hao, M.; Yang, X.; Sun, F.; Bai, Y.; Ding, H.; Wang, S.; Zhang, T. Sustainable and flexible hydrovoltaic power generator for wearable sensing electronics. *Nano Energy* **2020**, *72*, 104663.
(113) Saha, K.; Deka, J.; Raidongia, K. Extraction of Evaporation-Driven Electrokinetic Streaming Potential from V2O5 Nanochannels through Secondary Sources. *Acs Appl. Energ Mater.* **2021**, *4* (8), 8410−8420.
(114) Wang, Z.; Wu, Y.; Xu, K.; Jiang, L.; Sun, J.; Cai, G.; Li, G.; Xia, B. Y.; Liu, H. Hierarchical Oriented Metal−Organic Frameworks Assemblies for Water-Evaporation Induced Electricity Generation. *Adv. Funct. Mater.* **2021**, *31* (47), 2104732.
(115) Xiao, P.; He, J.; Ni, F.; Zhang, C.; Liang, Y.; Zhou, W.; Gu, J.; Xia, J.; Kuo, S.-W.; Chen, T. Exploring interface confined water flow and evaporation enables solar-thermal-electro integration towards clean water and electricity harvest via asymmetric functionalization strategy. *Nano Energy* **2020**, *68*, 104385.
(116) Li, J.; Liu, K.; Ding, T.; Yang, P.; Duan, J.; Zhou, J. Surface functional modification boosts the output of an evaporation-driven water flow nanogenerator. *Nano Energy* **2019**, *58*, 797−802.

https://doi.org/10.1021/acsami.4c09044
ACS Appl. Mater. Interfaces 2024, 16, 47050−47074

(117) Zhang, S.; Fang, S.; Li, L.; Guo, W. Geometry effect on water-evaporation-induced voltage in porous carbon black film. *Science China Technological Sciences* **2021**, *64* (3), 629−634.
(118) Wang, L.; Liu, L.; Solin, N. Ionovoltaic electricity generation over graphene-nanoplatelets: protein-nanofibril hybrid materials. *Nanoscale Adv.* **2023**, *5* (3), 820−829.
(119) Li, L.; Feng, S.; Bai, Y.; Yang, X.; Liu, M.; Hao, M.; Wang, S.; Wu, Y.; Sun, F.; Liu, Z.; et al. Enhancing hydrovoltaic power generation through heat conduction effects. *Nat. Commun.* **2022**, *13* (1), 1043.
(120) Lao, J.; Wu, S.; Gao, J.; Dong, A.; Li, G.; Luo, J. Electricity generation based on a photothermally driven Ti3C2Tx MXene nanofluidic water pump. *Nano Energy* **2020**, *70*, 104481.
(121) Dhiman, P.; Yavari, F.; Mi, X.; Gullapalli, H.; Shi, Y.; Ajayan, P. M.; Koratkar, N. Harvesting energy from water flow over graphene. *Nano Lett.* **2011**, *11* (8), 3123−3127.
(122) Yin, J.; Zhang, Z.; Li, X.; Zhou, J.; Guo, W. Harvesting Energy from Water Flow over Graphene? *Nano Lett.* **2012**, *12* (3), 1736−1741.
(123) Li, L.; Gao, S.; Hao, M.; Yang, X.; Feng, S.; Li, L.; Wang, S.; Xiong, Z.; Sun, F.; Li, Y. A novel, flexible dual-mode power generator adapted for wide dynamic range of the aqueous salinity. *Nano Energy* **2021**, *85*, 105970.
(124) Tabrizizadeh, T.; She, Z.; Stamplecoskie, K.; Liu, G. Empowerment of Water-Evaporation-Induced Electric Generators via the Use of Metal Electrodes. *ACS Omega* **2022**, *7* (32), 28275−28283.
(125) Xu, X.; Yang, X.; Zhang, Z.; Hong, Y.; Liu, S.; Shan, Y.; Peng, Z.; Wang, S.; Yao, X.; Yang, Z. Identification of metal−air batteries from water energy harvesters. *Droplet* **2023**, *2* (4), e80.
(126) Das, S. S.; Pedireddi, V. M.; Bandopadhyay, A.; Saha, P.; Chakraborty, S. Electrical Power Generation from Wet Textile Mediated by Spontaneous Nanoscale Evaporation. *Nano Lett.* **2019**, *19* (10), 7191−7200.
(127) Zheng, Y.; Liu, T.; Wu, J.; Xu, T.; Wang, X.; Han, X.; Cui, H.; Xu, X.; Pan, C.; Li, X. Energy Conversion Analysis of Multilayered Triboelectric Nanogenerators for Synergistic Rain and Solar Energy Harvesting. *Adv. Mater.* **2022**, *34* (28), 2202238.
(128) Wang, L.; Li, W.; Song, Y.; Xu, W.; Jin, Y.; Zhang, C.; Wang, Z. Monolithic Integrated Flexible Yet Robust Droplet-Based Electricity Generator. *Adv. Funct. Mater.* **2022**, *32* (49), 2206705.
(129) Oh, S.; Kim, K. J.; Goh, B.; Park, C. L.; Lee, G. D.; Shin, S.; Lim, S.; Kim, E. S.; Yoon, K. R.; Choi, C.; et al. Chemo-Mechanical Energy Harvesters with Enhanced Intrinsic Electrochemical Capacitance in Carbon Nanotube Yarns. *Adv. Sci.* **2022**, *9* (32), e2203767.
(130) Zheng, G.; Cui, Y.; Jiang, Z.; Zhou, M.; Yu, Y.; Wang, P.; Wang, Q. Fiber-based photothermal, UV-resistant, and self-cleaning coatings fabricated by silicon grafted copolymers of chitosan derivatives and gallic acid. *Int. J. Biol. Macromol.* **2022**, *222* (Pt A), 1560−1577.
(131) Zhang, Q.; Jiang, C.; Li, X.; Dai, S.; Ying, Y.; Ping, J. Highly Efficient Raindrop Energy-Based Triboelectric Nanogenerator for Self-Powered Intelligent Greenhouse. *ACS Nano* **2021**, *15* (7), 12314−12323.
(132) Qin, Y.; Wang, Y.; Sun, X.; Li, Y.; Xu, H.; Tan, Y.; Li, Y.; Song, T.; Sun, B. Constant Electricity Generation in Nanostructured Silicon by Evaporation-Driven Water Flow. *Angew. Chem., Int. Ed. Engl.* **2020**, *59* (26), 10619−10625.
(133) Liang, F.; Chao, X.; Yu, S.; Gu, Y.; Zhang, X.; Wei, X.; Fan, J.; Tao, X.-m.; Shou, D. An All-Fabric Droplet-Based Energy Harvester with Topology Optimization. *Adv. Energy Mater.* **2022**, *12* (9), 2102991.
(134) Zhong, T.; Guan, H.; Dai, Y.; He, H.; Xing, L.; Zhang, Y.; Xue, X. A self-powered flexibly-arranged gas monitoring system with evaporating rainwater as fuel for building atmosphere big data. *Nano Energy* **2019**, *60*, 52−60.
(135) Hu, S.; Shi, Z.; Zheng, R.; Ye, W.; Gao, X.; Zhao, W.; Yang, G. Superhydrophobic Liquid-Solid Contact Triboelectric Nanogenerator as a Droplet Sensor for Biomedical Applications. *ACS Appl. Mater. Interfaces* **2020**, *12* (36), 40021−40030.
(136) Han, K.; Zhang, D.; Zhuang, W.; Wan, Y.; Yang, P. Integrated multimodal microfluidic E-skin powered by synergistic tandem nanogenerators for sweat-based health monitoring and skin-temperature analysis. *J. Mater. Chem. A* **2023**, *11* (32), 17112−17124.

https://doi.org/10.1021/acsami.4c09044
ACS Appl. Mater. Interfaces 2024, 16, 47050−47074